

Point by point response to review#1

We are very thankful for the thorough review from which the manuscript benefited greatly. It allowed us to better work out the benefits and limitations of this study. The new benchmark proved to be very valuable to set the calibration results into context and to make a case for spatial ice sheet model calibrations. We believe we can address all concerns in a convincing manner, as outlined in the following.

Anonymous Referee #1

Received and published: 18 September 2019

This paper presents a new approach to probabilistic forecasting of future ice flow. [...] However I have serious concerns about the conclusions that the authors made from the application of their methods and cannot recommend the paper for publication. These methods have not yet been benchmarked on representative synthetic problems and this step is a necessary prerequisite for the publication of results using new methods.

We have now added a benchmark on representative synthetic problems as suggested, and adjusted our conclusions accordingly. This has allowed us to improve clarity on what we can, and what we cannot, achieve with this calibration approach, and how it compares to other approaches. Changes have been made throughout the manuscript but most notable are the new sections 3.5 (Calibration model test) and 3.6 (Comparison with other calibration approaches).

General comments:

The statistical methods that the authors use are comparatively new in glaciology. The authors cite several precedents from other fields and a paper by Chang and others from 2016 that used a similar combination of emulation and calibration. Chang et al 2016 and the current paper apply these methods to different datasets, however, and the success of the method at making certain inferences from one data set is no guarantee that the inferences from a different one are accurate.

To establish the correctness and capability of a new method on real data, it is common practice to first test it on a synthetic problem where the ground truth values of all fields and the signal-to-noise ratio of the synthetic observations are both known exactly. Without going through this preliminary testing step, you cannot be sure if the method improves on existing approaches, if the posterior density assigns non-zero probability to ground truth values, or even if the code to implement it is correct.

We agree and have now added a synthetic model test which we have applied to our proposed calibration approach as well to two other approaches for comparison. This analysis shows, very much in agreement with your remarks below, that the sliding law is not correctly inferred with any of the approaches tested here. The same is true for the ocean melt rate and we propose an explanation in the following (see below).

As the calibration does not adequately constrain these two parameters, we base the calibration only on the remaining parameters, namely the bedrock and basal traction and viscosity scalings. We use a uniform prior for basal melt and select nonlinear sliding by expert judgment (see below for reasoning).

The synthetic model test is described in section 3.5.

My most serious concern is with the authors' finding that a linear sliding relation gave the best fit to observational data using their calibration procedure. This result disagrees with recent published work using model-data comparison. Gillet-Chaulet et al. 2016 found that $m = 1/5$ or smaller gave the best fit to several years of velocity measurements for Pine Island Glacier. Joughin et al. 2019 tested the linear viscous, Weertman, and Schoof sliding laws against several years of velocity and thickness change measurements at Pine Island Glacier and found that the Schoof sliding law, which is asymptotic to $m = 0$ in the limit of high sliding speed, gave the best fit to observations. Other studies through the years have found evidence for nonlinear sliding using methods ranging from laboratory studies to seismic sensing. The authors state that their calibration procedure gave the best fit with $m = 1$ with little further discussion. Is this an assertion that glacier sliding really is linear viscous, despite numerous studies showing nonlinear and even near-plastic sliding? Or is it an artifact of the calibration? If it's the latter then the calibration procedure should be fixed, as other published methods do not come to this same conclusion.

Agreed, as explained above, the preference to linear sliding was not a robust finding. We follow your argument to justify the selection of nonlinear sliding by expert judgment.

“From this test we conclude that basal sliding law and ocean melt scaling cannot be inferred from this calibration approach. We will therefore only calibrate the bedrock as well as basal traction and viscosity scaling factors. Several studies used the observed dynamical changes of parts of the ASE to test different sliding laws. Gillet-Chaulet et al. (2016) find a better fit to evolving changes of Pine Island Glacier surface velocities for smaller m , reaching a minimum of the cost function from around $m=1/5$ and smaller. This is supported by Joughin et al. (2019) who find $m=1/8$ to capture the PIG speed up from 2002 to 2017 very well, matched only by a regularized Coulomb (Schoof-) sliding law. It further is understood that parts of the ASE bed consist of sediment-free, bare rocks for which a linear Weertman sliding law is not appropriate (Joughin et al., 2009). We therefore select nonlinear sliding by expert judgment and use a uniform prior for the ocean melt scaling.”

Moreover, the finding that $m = 1$ gave the best fit to observations compared to other parameter choices that were tried does not imply that it gives a good fit to observations in any absolute sense. If the errors in the thickness change measurements are, for example, normally distributed with known variance, then the normalized sum of squared errors should come out to around 1/2. The Konrad et al 2017 paper only offers some range of possible measurement errors but this could be handled in a hierarchical Bayesian framework and the idea is the same. The question is not just what parameter combination gave the best fit to observations, but also whether that fit is good enough in an absolute sense given what we know about the error statistics. Otherwise we are merely choosing the best among bad options. This issue is discussed in MacAyeal et al. 1995 and Habermann et al. 2012.

This issue is now addressed by an initial history matching where for each parameter combination the implausibility parameter is calculated and only those parameter combinations with an implausibility below a threshold based on 95% of a chi-squared distribution with k degrees of freedom are considered for the probabilistic calibration. This initial history matching ensures that the probabilistic calibration is only based on parameter combinations which are sufficiently close to the observations that they cannot be easily ruled out. About 1.4% of the input space cannot be ruled out in this way.

This is now covered in the new section 3.4.1: History matching

Part of the problem might stem from the choice of which parameters to calibrate. The only means by which the viscosity and basal traction can be adjusted is by scaling the amplitude of the optimal results from an inversion computed in Nias et al. 2016. The emulation method can capture the sensitivity of model outputs to variations in this amplitude scaling, but amplitude scaling as such is not necessarily a good way to capture additional modes of spatial variability. Several papers (Isaac et al. 2015, Petra et al. 2014) have successfully applied a dimensionality reduction approach in inverse problems by using the largest several eigenvalues of the Gauss-Newton approximation to the Hessian of the log-posterior. The unusual results from the calibration procedure might be ameliorated by a different choice of basis.

We agree that scaling an optimized input field, as has been done for the dataset used here, is inferior to fully exploring the ice sheet response to more flexible, higher dimensional variations to the input fields. However, computational and methodological challenges make simple scaling approaches more feasible and a common approach to represent basal traction coefficient uncertainty in forward ice sheet model simulations (see e.g. Schlegel et al. 2018, Nias et al. 2019). That is, if this uncertainty is represented at all.

The focus of this manuscript is on how spatial observations can be used for calibration of an existing set of ice sheet model simulations. Here it is not our intention to improve the initial design of ensemble experiments. Therefore higher dimensional perturbations are not possible in this case. This focus has been clarified, e.g. by the following paragraph:

“The model perturbation has been done by amplitude scaling of the optimized input fields alone, other variations to the input fields could potentially produce model setups with better agreement to the observations (Petra et al., 2014; Isaac et al., 2015). However, computational and methodological challenges make simple scaling approaches more feasible and the use of a published dataset bars us from testing additional types of perturbations. Probabilistic calibrations are an assessment of model setups to be the best of all tested cases. It has to be clear that this is, despite emulation, a vast simplification in searching for the best of all possible model setups imaginable.”

Schlegel, Nicole-Jeanne, et al. "Exploration of Antarctic Ice Sheet 100-year contribution to sea level rise and associated model uncertainties using the ISSM framework." *Cryosphere* 12.11 (2018): 3511-3534.

Nias, I. J., et al. "Assessing uncertainty in the dynamical ice response to ocean warming in the Amundsen Sea Embayment, West Antarctica." *Geophysical Research Letters*. (2019)

Finally, the authors state that the prediction uncertainty is greatly reduced by using their method. However, they apply a constant climate forcing, which is difficult to justify given recent trends of CO2 release that more follow the RCP8.5 scenario. The authors also state that future ocean warming is uncertain, but recent results from ocean GCMs suggest that the warming trend around the Amundsen Sea is likely to continue into the future, see Holland et al. 2019.

We agree that the simulations used here should not be understood as predictions and we have made this more clear in the manuscript now. We are not using the word ‘prediction’ for the model simulations used here anymore. We also take up the findings of Holland et al. 2019 but it has to be clear that it is one thing to suggest a long-term anthropogenic influence on the ocean melt in the

ASE and a very different challenge to robustly represent climate scenarios in model simulations. To quote Holland et al. (2019):

“Owing to the unpredictable phasing of internal climate variability, there is significant variance in wind trends between ensemble members, with the 1 s.d. range for LENS and MENS extending between no trend and twice the mean trend (Supplementary Fig. 6). Internal variability is therefore of comparable importance to radiative forcing in determining the magnitude of PITT wind changes during the twenty-first century. In the CMIP5 ensembles, inter-model differences add further uncertainty to the future trajectory of PITT winds (Supplementary Fig. 6). To deliver meaningful projections of the WAIS over this period, ice-sheet models will need to adopt an ensemble approach forced by multiple realizations of ocean melting.”

Note that our projections are even shorter than the time scales considered in the quote, increasing the role of internal variability even more.

We therefore note that climate scenarios are expected to have small net impact on 50 year simulations and add:

“Relating climate scenarios to local ice shelf melt rates is associated with deep uncertainties itself. CMIP5 climate models are inconsistent in predicting Antarctic shelf water temperatures so that the model choice can make a substantial (>50%) difference in the increase of ocean melt by 2100 for the ASE (Naughten et al., 2018). Melt parameterisations, linking water temperature and salinity to ice melt rates, can add variations of another 50% in total melt rate for the same ocean conditions (Favier et al., 2019). The location of ocean melt can be as important as the integrated melt of an ice shelf (Goldberg et al., 2019). The treatment of melt on partially floating grid cells further impacts ice sheet models significantly, even for fine spatial resolutions of 300 m (Yu et al., 2018). It is therefore very challenging to make robust climate scenario dependent ice sheet model predictions. Instead we use projections of the current state of the ASE for a well defined set of assumptions for which climate forcing uncertainty is simply represented by a halving to doubling in ocean melt.”

Naughten, Kaitlin A., et al. "Future projections of Antarctic ice shelf melting based on CMIP5 scenarios." *Journal of Climate* 31.13 (2018): 5243-5261.

Favier, L., Jourdain, N. C., Jenkins, A., Merino, N., Durand, G., Gagliardini, O., Gillet-Chaulet, F., and Mathiot, P. (2019). Assessment of sub-shelf melting parameterisations using the ocean–ice-sheet coupled model nemo (v3. 6)–elmer/ice (v8. 3). *Geoscientific Model Development*, 12(6):2255–2283.

Yu, Hongju, et al. "Retreat of Thwaites Glacier, West Antarctica, over the next 100 years using various ice flow models, ice shelf melt scenarios and basal friction laws." *The Cryosphere* 12.12 (2018): 3861-3876.

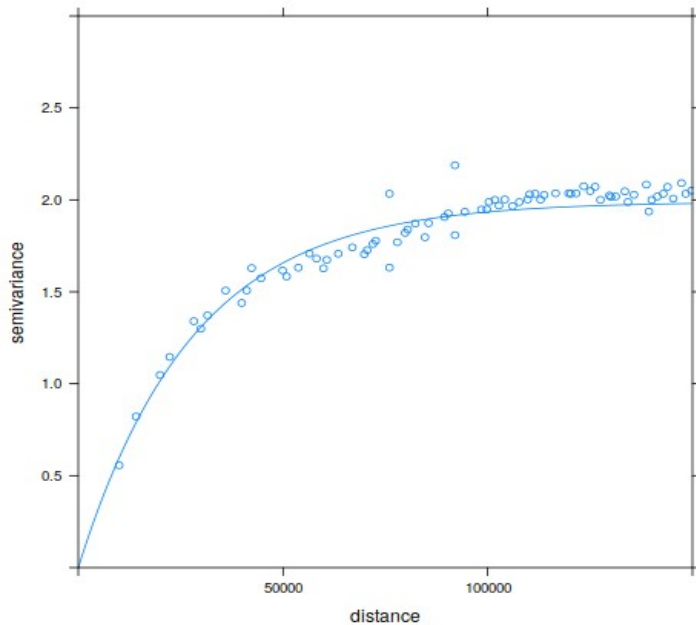
In general the study has been re-framed towards a methods test which reduces the importance of the SLR projections.

Specific comments:

Page 2: 10-11: Worth mentioning some of the paleoglaciology literature, see Hein et al. 2016.

Done

Page 3: 9-11: How nearby and how correlated? A standard approach in geostatistics would be to assume that the correlations between the error made in measurements at point x and point y is proportional to $\exp(-|x - y|/L)$ for some correlation length L . What is the correlation length for the observational data you're using? You assert that model-to-observation comparisons on a cell-by-cell basis are not statistically independent, but that depends on whether the model resolution is large or small compared to the correlation length.



Using the seven year mean, gridded (10X10km) dh/dt data from Konrad et al. (2017) for the ASE we derived the above semivariogram which has a range value for the shown exponential fit of approximately 28000 m. Therefore the covariance of measurements 28km apart from each other reaches about 63% of the far field variance (the sill = $2 \text{ m}^2 \text{ year}^{-2}$). This is in agreement with visual inspections for Figure 1 of Konrad et al. (2017) and means that $L > 10\text{km}$. This has been added to the supplement.

Page 4: 15-16: Why should scaling the viscosity and friction coefficients up and down be a good way to capture variability in these fields that was not captured in the original study by Nias et al.? The true misfit might instead have a completely different spatial pattern.

The model ensemble, including the scaling, is performed by Nias et al. (2016). See above discussion on the use of scaling factors

Page 10: 3: The fact that the most likely fields match the inversion from Nias only tells us that the fit can't be improved within the much lower-dimensional parameter space that you've chosen, not that it can't be improved through the addition of a completely different mode of spatial variability.

We did not intend to claim that there cannot be further improvements. The referenced note about "suggested good model consistency" was directed towards the absence of basin wide velocity

biases, which could be balanced by scaled traction or viscosity fields. However, we removed this statement.

References:

Gillet-Chaulet et al. 2016, Assimilation of surface velocities acquired between 1996 and 2010 to constrain the form of the basal friction law under Pine Island Glacier, Geophysical Research Letters

Habermann et al. 2012, Reconstruction of basal properties in ice sheets using iterative inverse methods, Journal of Glaciology

Hein et al. 2016, Evidence for the stability of the West Antarctic Ice Sheet Divide for 1.4 million years, Nature communications.

Holland et al. 2019, West Antarctic ice loss influenced by internal climate variability and anthropogenic forcing, Nature Geoscience.

Isaac et al. 2015, Scalable and efficient algorithms for the propagation of uncertainty from data through inference to prediction for large-scale problems, with application to flow of the Antarctic ice sheet, Journal of Computational Physics

Joughin et al. 2019, Regularized Coulomb Friction Laws for Ice Sheet Sliding: Application to Pine Island Glacier, Antarctica, Geophysical Research Letters

MacAyeal et al. 1995, Basal friction of Ice Stream E, West Antarctica, Journal of Glaciology.

Petra et al. 2014, A Computational Framework for Infinite-Dimensional Bayesian Inverse Problems, Part II: Stochastic Newton MCMC with Application to Ice Sheet Flow Inverse Problems, SIAM Journal of Scientific Computing

MacAyeal et al. 1995, Basal friction of Ice Stream E, West Antarctica, Journal of Glaciology.

Petra et al. 2014, A Computational Framework for Infinite-Dimensional Bayesian Inverse Problems, Part II: Stochastic Newton MCMC with Application to Ice Sheet Flow Inverse Problems, SIAM Journal of Scientific Computing

References have been added.

Point by point response to review#2

We are very thankful for the thorough review from which the manuscript benefited greatly. In particular we hope that the stronger focus on method evaluation instead of future sea level/retreat might increase the value of the manuscript for the wider ice sheet modelling community. We believe we can address all concerns in a convincing manner, as outlined in the following.

In the manuscript, Wernecke et al., present a promising method to calibrate uncertainty distributions of mass loss derived from ice-sheet model simulations with spatial data. [...] Before considering it for publication, I recommend additional analyses, a more detailed discussion of the capabilities and limitations of the method and reframing as explained in the comments below.

Major comments:

- *p.1 l.9, l.11, & other: with some more analysis, this study can make a very good test case that demonstrates the capabilities of the new method. However, it is problematic to say that in this study you are estimating future sea-level contribution or that you are making ‘predictions’ or ‘projections’, since your analysis is based on simulations with constant ocean forcing, excluding for example natural variability (e.g., Jenkins et al., 2016) or potential future changes in ambient oceanic and atmospheric conditions (e.g., Holland et al., 2019) depending on the different socio-economic pathways (RCP scenarios). Possible future evolution of surface mass balance is not considered and uncertainty in basal melting is based on a simple amplitude scaling, neglecting for instance the effect of changes in spatial melt rate distributions (discussed, e.g., in Goldberg et al., 2019) or uncertainties related to the basal melt rate parameterisation (see, e.g., Favier et al., 2019).*

We agree that we should have been more clear about the limitations of our projections. As suggested, the revised manuscript now focuses on testing the method.

We are not using the word ‘prediction’ for the model simulations used here any more. We also note that climate scenarios are expected to have small net impact on 50 year simulations and add:

“Relating climate scenarios to local ice shelf melt rates is associated with deep uncertainties itself. CMIP5 climate models are inconsistent in predicting Antarctic shelf water temperatures so that the model choice can make a substantial (>50%) difference in the increase of ocean melt by 2100 for the ASE (Naughten et al., 2018). Melt parameterisations, linking water temperature and salinity to ice melt rates, can add variations of another 50% in total melt rate for the same ocean conditions (Favier et al., 2019). The location of ocean melt can be as important as the integrated melt of an ice shelf (Goldberg et al., 2019). The treatment of melt on partially floating grid cells further impacts ice sheet models significantly, even for fine spatial resolutions of 300 m (Yu et al., 2018). It is therefore very challenging to make robust climate scenario dependent ice sheet model predictions. Instead we use projections of the current state of the ASE for a well defined set of assumptions for which climate forcing uncertainty is simply represented by a halving to doubling in ocean melt.”

Naughten, Kaitlin A., et al. "Future projections of Antarctic ice shelf melting based on CMIP5 scenarios." *Journal of Climate* 31.13 (2018): 5243-5261.

Favier, L., Jourdain, N. C., Jenkins, A., Merino, N., Durand, G., Gagliardini, O., Gillet-Chaulet, F.,

and Mathiot, P. (2019). Assessment of sub-shelf melting parameterisations using the ocean–ice-sheet coupled model nemo (v3. 6)–elmer/ice (v8. 3). *Geoscientific Model Development*, 12(6):2255–2283.

Yu, Hongju, et al. "Retreat of Thwaites Glacier, West Antarctica, over the next 100 years using various ice flow models, ice shelf melt scenarios and basal friction laws." *The Cryosphere* 12.12 (2018): 3861-3876.

We thus argue that due to the large and multi-level uncertainty in RCP forced simulations the simple ocean melt scaling can be considered a representation of climate forcing uncertainty. This is not to say that we predict the future but that we do not neglect uncertainty in the forcing altogether. As long as we are not able to robustly propagate uncertainties through every level of the mapping from climate scenarios to sub-ice shelf melt, we consider a simple perturbation approach most appropriate.

In general the manuscript is re-framed towards a methods test, by adding a new synthetic model test and comparisons with different calibration approaches. This further reduces focus from the SLR projections. The spatial retreat probabilities section has been removed.

• *p.5 l.11: the choice of calibration of dh/dt after running the model for 7 years appears random. Please explain this. Also, how would your results be influenced if your calibration was done after 1, 5 or 10 years?*

The rationale to use dh/dt fields for calibration is the following. The variety of datasets available to calibrate ice sheet models is limited. Reliable and spatially-resolved satellite observations which could be useful for calibrations are limited to surface ice velocity, surface elevation and the corresponding rates of change. The surface velocity is used for model inversion and is therefore not an independent parameter. The absolute ice thickness (equivalent to using ice surface elevation with a fixed bedrock) is also set in the model parameter inversions and in addition only semi-continuous (as it cannot become negative). This causes additional challenges as described in Chang et al. (2019). We avoid these challenges by using ice thickness change data (which can be considered fully continuous as long as changes in ice thickness are smaller than the total thickness so that negative and positive values are equally possible).

Regarding the period, we compare several calibration periods and find a short spin-up phase of three years to be beneficial. Following this spin-up, the proposed calibration approach on the first four years, seven years and from the fourth to the seventh year all produce very similar results with projections for the end of model period of 21 [16.8, 25.5], 19.1[13.9, 24.8] and 19.5 [15.9, 24.4] mm SLE (weighted mean and 5.- and 95- percentiles), respectively. In the spin-up period the model adjusts to the boundary conditions and calibrating on this period with the proposed approach creates a tendency towards slower ice sheet model runs and an underestimation of sea level contribution. The analysis has been changed accordingly and the sensitivities to the calibration period is now discussed in the manuscript with more information the the supplement.

Chang, Won, et al. "Ice Model Calibration Using Semi-continuous Spatial Data." *arXiv preprint arXiv:1907.13554* (2019).

• *p.12 l.3: my understanding of Nias et al. (2016) is, that inversion techniques were used to estimate the spatial fields of viscosity and basal traction coefficients. Were different inversions run for the different bed geometries and values of m ? If the inversion was run only for $m = 1$, a better fit for $m = 1$ in comparison to $m = 1/3$ would not be a surprise as*

the parameter fields were optimized for this case. If this is true, your findings are maybe more due to the experimental design rather than being physically interpretable. Please clarify this (similar for the bed topography and the other parameters) and, if applicable, consider it in the discussion of your findings.

Thank you for the suggestion. However, Nias et al. (2016) used different basal traction coefficient fields for the different sliding laws and bed geometries. This has been clarified in the manuscript.

- *p.14 l.24-27 and Appendix B: you state that your method improves calibration with aggregated variables. It is interesting to see the effect on the different parameters (Figure B1), but to make this point clear, please add also the effect on the mass loss and grounding line probability estimates (similar to Figures 5,6).*

We now address the impact of different calibration approaches in much more detail. This is done on a synthetic model test (new section 3.6), likelihood estimates (supplement) and for projections of mass loss (Figure 4).

Further comments:

- *page 2 lines 22ff: there are a number of modelling studies with coarser resolution that do not require a parameterised grounding line for retreat (e.g., Schlegel et al., 2018). ‘Regional’ is maybe more appropriate than ‘one glacier’ (e.g. Arthern and Williams, 2017).*

We tried to clarify that we are talking about challenges of adequate representations of the grounding line in low resolution models in general and make sure not to imply that there are no useful low resolution model studies without sub-resolution parameterisation. We also follow the suggestion of using ‘regional’.

“In most studies, the computational expense of exploring uncertainties either restricts the minimum spatial resolution to several kilometres, causing challenges in representing the grounding line, or else are restricted regional applications.”

- *p.2 l.28 and l.20: please check your use of ‘predicted’ versus ‘projected’.*

We do not use ‘predictions’ for the model simulations used in this study any more.

- *p.3 l.23-29: emulation of model output was also used for example in Levermann et al. (2014).*

Corrected

- *p.4 section 2.1: since basal melt is the driver of mass loss in the Amundsen Sea at present, more details should be given here, e.g., how do mass fluxes compare to observations?*

We added:

“The ensemble covers a wide range of sea level rise contributions for the 50 year period with the most extreme members reaching -0.19 mm/year and 1.62 mm/year, respectively. About 10% of the ensemble shows an increasing volume above flotation (negative sea level contribution) and the central runs (0.5 for traction, viscosity and ocean melt parameters) contribute 0.27 mm/year (linear sliding) and 0.26 mm/year (nonlinear sliding). The average contributions are generally reasonably close to satellite observations (0.33 ± 0.05 mm/year from 2010-2013 (McMillan et al., 2014)) with 0.30 mm/year for linear sliding and modified bedrock, 0.37 mm/year for linear sliding and Bedmap-2, 0.38 mm/year for nonlinear sliding and modified bedrock and 0.51 mm/year for nonlinear sliding and Bedmap-2 (Nias et al., 2016).

• p.5 l.13: you could state here that your $y(\theta_i)$ is dhdt.

Done

• p.5 l.16: $\Theta = [0, 1]^5 \subseteq \mathbb{R}^d$?

Clarified

• p.5 l.21: shouldn't $S \in \mathbb{R}^{m \times n}$, $U \in \mathbb{R}^{m \times m}$, $V \in \mathbb{R}^{n \times n}$, since U, V are unitary matrices and by definition quadratic? Please check also the other matrix dimensions.

You are right, we got sidetracked by S being diagonal but not square. Thank you.

• Section 3.1: a reference to Fig. 1 is missing.

Added

• Figure 1: please give here more explanation, e.g., of 'unit length'.

Replaced 'unit length' by "normalized PCs, building an orthogonal basis" and explain: "They represent the main modes of variation in the model ensemble"

• p.6, l.8: would it be an option to calibrate not only after 7 years but at all datasets from Konrad et al. (2017) individually as they find variations in the onset and propagation of surface lowering?

A spatio-temporal calibration would be a logical next step and is now mentioned in the discussion, but we believe this would exceed the scope of this study.

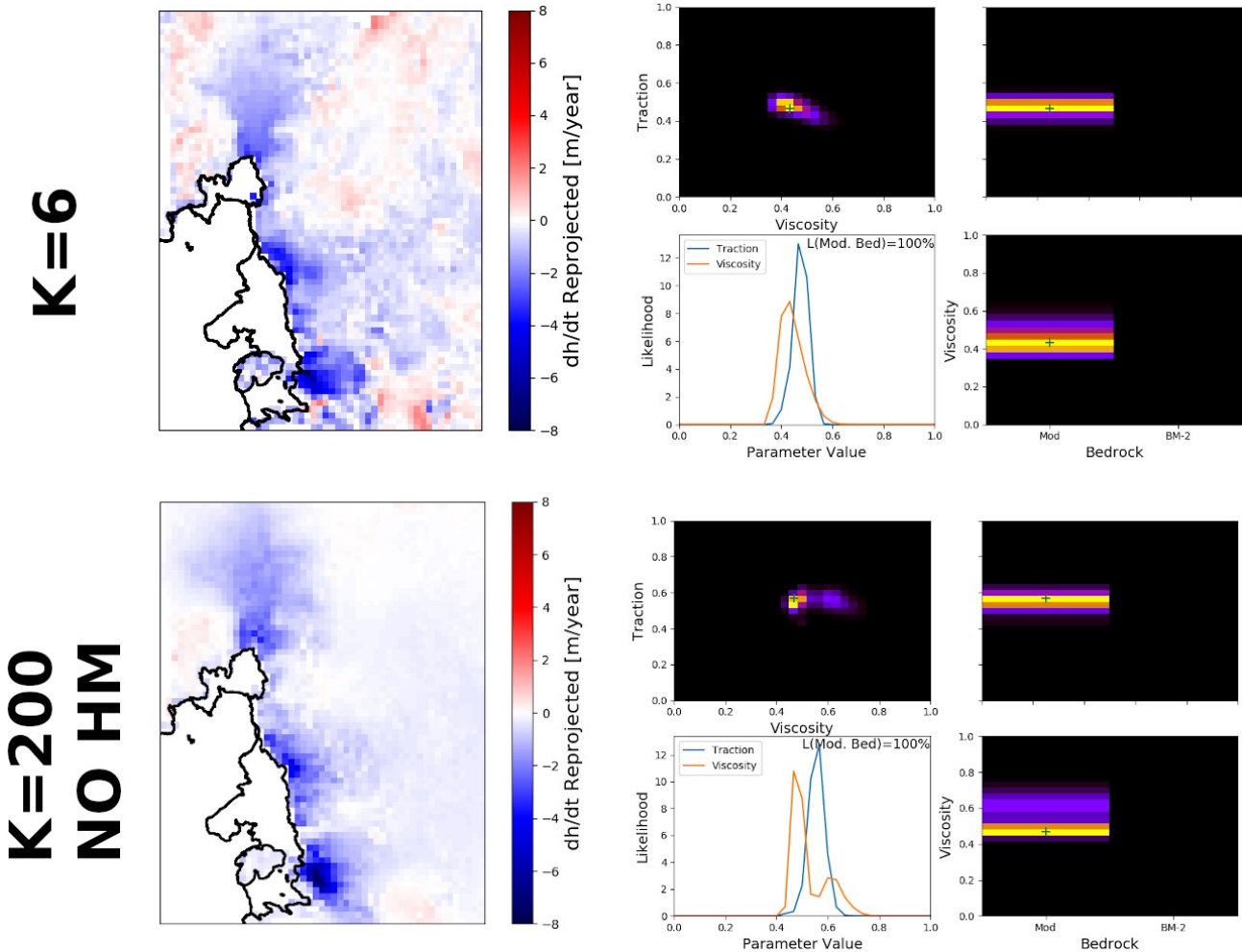
• Figure 2: in your reprojection of the mean observation, artifacts of thickening occur. How will this affect your calibration?

• p.7 l.1: a value of 0.6 seems to be rather large, please explain.

Combined:

By increasing the truncation value k we can investigate how said artifacts influence the calibration. For values of k greater than six the whole parameter space is ruled out by history matching. As can be seen, increasing k to six does not remove the positive artifacts and the likelihood distribution does change only marginally (compare upper right quarter of the figure below with Figure 5a in the manuscript).

Therefore we turn the history matching off to investigate the behaviour for large k . The positive artifacts disappear for large values of k (e.g. $k=200$) and the fraction of the observations which cannot be represented by k principal components, as evaluated by the remaining spatial variance, reduces from 0.58 to 0.09. The likelihood distribution is affected but the overall picture is the same (compare top to bottom of following Figure). This includes a fair amount of overlap of the more likely parameter setups. We conclude that the influence of the artifacts is small.



Caption: Re-projected mean observations (left) and likelihood distribution (right) for truncation value $k=6$ (top) and $k=200$ (bottom).

- p.7 l. 5: I cannot find where this is discussed in the results section?

It was not discussed but the BISICLES ensemble runs are now added as histogram in the SLE distribution plot to illustrate the improved representation by using emulation. This is now also mentioned in the text.

- p.7 l.7: you could help the reader if you explain what the rows of $S^0 T^0 T$ represent.

Done:

“A row of $V^{\wedge}T$ can be understood as indices of how much of a particular principal component is present in every ice sheet model simulation.”

- p.7 l.7: how is the training done? please give more details here.
- p.7 l.12: I cannot find the definition of a Gaussian Process Emulator in the given reference.
- p.7 l.15ff: more details are needed here.

Combined:

We now additionally feature Equation 2.19 from Rasmussen and Williams (2006) in the manuscript which describes in detail how the emulator predictions are based on the training data and hence how to understand the training process. In this context more details are also added to the description of the covariance function and how exactly it is used. We also reference the python functions which are used for training and marginal likelihood optimization.

• p.8 l.16: eqn.3

corrected

• Section 3.4: you are switching between observational errors and model errors in this section. It might be easier to read if you give and explain one by one.

Has been rearranged

• p.10 l.11: prediction, see above

Corrected

• p.15 l. 28: 'the' too much

Corrected

• p.16 l. 4: please specify 'uniform within the parameter space'.

Rephrased:

"The emulator performance, as described above, shows no dependence on the input parameters"

• Figure A2: how are the quantities shown on the x and y axis obtained?

We expanded the description and added the mathematical nomenclature used elsewhere.

• Appendix B: It would be great to see also how your method compares to calibrations using a spatially aggregated, temporal evolution of mass loss as used for example for targeted parameter optimization in Golledge et al. (2019).

We increased the use of spatially aggregated quantities to compare the calibrations but think that a temporal calibration would exceed the scope of this manuscript.

References

Arthern, R. J. and Williams, C. R. (2017). The sensitivity of west antarctica to the submarine melting feedback. *Geophysical Research Letters*, 44(5):2352–2359.

Favier, L., Jourdain, N. C., Jenkins, A., Merino, N., Durand, G., Gagliardini, O., Gillet-Chaulet, F., and Mathiot, P. (2019). Assessment of sub-shelf melting parameterisations using the ocean–ice-sheet coupled model nemo (v3. 6)–elmer/ice (v8. 3). *Geoscientific Model Development*, 12(6):2255–2283.

Goldberg, D., Gourmelen, N., Kimura, S., Millan, R., and Snow, K. (2019). How accurately should we model ice shelf melt rates? *Geophysical Research Letters*, 46(1):189–199.

Golledge, N. R., Keller, E. D., Gomez, N., Naughten, K. A., Bernales, J., Trusel, L. D., and Edwards, T. L. (2019). Global environmental consequences of twenty-first-century ice-sheet melt. *Nature*, 566(7742):65.

Holland, P. R., Bracegirdle, T. J., Dutrieux, P., Jenkins, A., and Steig, E. J. (2019). Climate forcing of the west antarctic ice sheet: Anthropogenic trends and internal climate variability. *Nature Geoscience*.

Jenkins, A., Dutrieux, P., Jacobs, S., Steig, E. J., Gudmundsson, G. H., Smith, J., and Heywood, K. J. (2016). Decadal ocean forcing and antarctic ice sheet response: Lessons from the amundsen sea. *Oceanography*, 29(4):106–117.

Konrad, H., Gilbert, L., Cornford, S. L., Payne, A., Hogg, A., Muir, A., and Shepherd, A. (2017). Uneven onset and pace of ice-dynamical imbalance in the amundsen sea embayment, west antarctica. *Geophysical Research Letters*, 44(2):910–918.

Levermann, A., Winkelmann, R., Nowicki, S., Fastook, J. L., Frieler, K., Greve, R., Hellmer, H. H., Martin, M. A., Meinshausen, M., Mengel, M., et al. (2014). Projecting antarctic ice discharge using response functions from searise ice-sheet models. *Earth System Dynamics*, 5(2):271–293.

Nias, I. J., Cornford, S. L., and Payne, A. J. (2016). Contrasting the modelled sensitivity of the amundsen sea embayment ice streams. *Journal of Glaciology*, 62(233):552–562.

Schlegel, N.-J., Seroussi, H., Schodlok, M. P., Larour, E. Y., Boening, C., Limonadi, D., Watkins, M. M., Morlighem, M., and Broeke, M. R. (2018). Exploration of antarctic ice sheet 100-year contribution to sea level rise and associated model uncertainties using the issm framework. *The Cryosphere*, 12(11):3511–3534.

All new references have been added to the manuscript

Spatial probabilistic calibration of a high-resolution Amundsen Sea Embayment ice-sheet model with satellite altimeter data

Andreas Wernecke¹, Tamsin L. Edwards², Isabel J. Nias^{3,4}, Philip B. Holden¹, and Neil R. Edwards¹

¹School of Environment, Earth and Ecosystem Sciences, The Open University, Milton Keynes, UK

²Department of Geography, King's College London, London, UK

³Earth System Sciences Interdisciplinary Center, University of Maryland, College Park, MD, USA

⁴Cryospheric Sciences Laboratory, NASA Goddard Space Flight Center, Greenbelt, MD, USA

Correspondence: Andreas Wernecke (andreas.wernecke@open.ac.uk)

Abstract.

Probabilistic predictions of the sea level contribution from Antarctica often have large uncertainty intervals. Calibration with observations can reduce uncertainties and improve confidence in projections, particularly if this exploits as much of the available information as possible (such as spatial characteristics), but the necessary statistical treatment is often challenging and can be computationally prohibitive. Ice sheet models with sufficient spatial resolution to resolve grounding line evolution are also computationally expensive.

Here we address these challenges by adopting a novel dimension-reduced approach to calibration, combined with statistical emulation of the adaptive mesh model BISICLES. ~~We find the most likely contribution to global mean sea level rise from~~ With the help of a published perturbed parameter ice sheet model ensemble of the Amundsen Sea Embayment (ASE) ~~over the next~~, we show how the use of spatially resolved observations can improve probabilistic calibrations. In synthetic model experiments (calibrating the model with altered model results) we can identify the correct basal traction and ice viscosity scaling parameters as well as the bedrock map with spatial calibrations while a net sea level contribution calibration imposes only weaker constraints.

Projections of the 50 years is 10.4 year sea level rise contribution from the current state of the ASE can be narrowed down with satellite observations of recent ice thickness change to 18.9 [0.6, 23.3] 13.9, 24.8 mm (mode and 5-95% probability interval), a substantial reduction in uncertainty from the uncalibrated estimates of 9.6 mm (median and 90% range) with the proposed spatial calibration approach, compared to 16.8 [-5.9, 78.2] 7.7, 25.6 mm. We predict retreat of the grounding line along most parts of the ASE coast with high confidence, with a maximum inland extent of around 28 km at Smith Glacier. The for the net sea level calibration and 23.1 [-8.4, 94.5] for the uncalibrated ensemble. The spatial model behaviour is much more consistent with observations if, instead of Bedmap2, a modified bedrock topography is used that most notably removes a topographic rise near the initial grounding line of Pine Island Glacier, though this does influence the future mass loss less than basal traction and viscosity scaling parameters.

The ASE dominates the current Antarctic sea level contribution, but other regions have the potential to become more important on centennial scales. These larger spatial and temporal scales would benefit even more from methods of fast but exhaustive model calibration. Our approach therefore has the potential to improve projections for the Antarctic ice sheet on continental and

centennial scales by efficiently improving our understanding of model behaviour, and substantiating and reducing projection uncertainties.

Copyright statement. Will be included by Copernicus

5 1 Introduction

The Antarctic ice sheet is currently losing mass at a rate of around 0.5 to 0.6 mm/year sea level equivalent, predominantly in the Amundsen Sea Embayment (ASE) area of the West Antarctic Ice Sheet (WAIS) (Shepherd et al., 2018; Bamber et al., 2018). This is due to the presence of warm Circumpolar Deep Water causing sub-shelf melting and ice dynamical changes including retreat of the grounding line that divides grounded from floating ice (Khazendar et al., 2016). The dynamical changes are consistent with those expected from the Marine Ice Sheet Instability (MISI) hypothesis (Favier et al., 2014; Ritz et al., 2015). Although projections of future ocean changes are uncertain, basal melting is expected to continue for the next few years to decades, possibly even if the external oceanic heat flux towards the ice sheet decays (Naughten et al., 2018). Persistent grounding line retreat could lead eventually to a collapse of the marine-based WAIS, contributing up to 3.4 m equivalent to global mean sea level (Fretwell et al., 2013) even though there are indications that a small part of the WAIS, centered at the Ellsworth Mountains, existed at least for the last 1.4 million years (Hein et al., 2016). However, the future response of the Antarctic ice sheet is one of the least well understood aspects of climate predictions (Church et al., 2013). Predictions of the dynamic ice sheet response are challenging because local physical properties of the ice and the bedrock it is laying on are poorly observed. Parameterisations of unresolved physical processes are often used and need to be validated (DeConto and Pollard, 2016; Edwards et al., 2019; Cornford et al., 2015; Pattyn et al., 2017). Progress has been made in the understanding of ice sheet feedbacks, like MISI and the Marine Ice Cliff Instability hypothesis (DeConto and Pollard, 2016), as well as the development of numerical models with higher resolutions and improved initialization methods (Pattyn, 2018). But these improvements cannot yet overcome the challenges of simulating what can be described as under-determined system with more unknowns than knowns. For this reason, some studies use parameter perturbation approaches which employ ensembles of model runs, where each ensemble member is a possible representation of the ice sheet using a different set of uncertain input parameter values (Nias et al., 2016; DeConto and Pollard, 2016; Schlegel et al., 2018; Gladstone et al., 2012; Ritz et al., 2015; Bulthuis et al., 2019) (Here we do not distinguish between initial values of state variables, which will change during the simulation, and model parameters, which represent physical relationships. All of those quantities can be poorly known and contribute to uncertainties in predictions.). In most studies, the computational expense of exploring uncertainties either restricts the minimum spatial resolution to several kilometres, ~~necessitating parameterisation of grounding lineretreatcausing~~ challenges in representing the grounding line, or else ~~restricts the domain to a single glacier~~ are restricted regional applications.

One exception is the ensemble by Nias et al. (2016), which uses the adaptive mesh model BISICLES at sub-km minimum resolution over the ASE domain (Pine Island, Thwaites, Smith and Pope glaciers).

In Antarctic ice sheet model ensemble studies, the projected sea level contribution by the end of the century typically ranges from around zero to tens of centimetres, i.e. the ensemble spread is twice the predicted (mean/median) contribution (Edwards et al., 2019). It is therefore essential to constrain ice sheet model parameters to reduce these uncertainties i.e. to attain sharper and more distinctive prediction distributions for different climate scenarios. Statistical calibration of model parameters refines predictions by using observations to judge the quality of ensemble members, in order to increase confidence in, and potentially reduce uncertainty in, the predicted distributions. Calibration approaches range from straightforward ‘tuning’ to formal probabilistic inference. Simple ruled out/not ruled out classifications (also called history matching or precalibration) can be used to identify and reject completely unrealistic ensemble members while avoiding assumptions about the weighting function used for the calibration (e.g. Holden et al., 2010; Williamson et al., 2017; Vernon et al., 2010). Formal probabilistic, or Bayesian, calibrations using high dimensional datasets require experience of statistical methods and can be computationally prohibitive (Chang et al., 2014). There are few ice sheet model studies using calibrations, among which are history matching (DeConto and Pollard, 2016; Edwards et al., 2019), gradual weight assignments (Pollard et al., 2016) and more formal probabilistic treatments (Ritz et al., 2015; Chang et al., 2016b, a). Most use one or a small number of aggregated summaries of the observations, such as spatial and/or temporal averages, thus discarding information that might better constrain the parameters.

Ideally, then, calibrating a computer model with observations should use all available information, rather than aggregating the observations with spatio-temporal means. However, the formal comparison of model simulations with two-dimensional observations, such as satellite measurements of Antarctica, poses statistical challenges. Measurements of the [Earth-earth](#) system typically show coherent spatial patterns, meaning that nearby observations are highly correlated due to the continuity of physical quantities. Model to observation comparisons on a grid-cell-by-grid-cell basis can therefore not be treated as statistically independent. On the other hand, appropriate treatment of these correlations with the inclusion of a co-variance matrix in the statistical framework for calibration can be computationally prohibitive (Chang et al., 2014). While the simplest way to avoid this is by aggregation, [often into a single value either over the whole domain](#) (Ritz et al., 2015; DeConto and Pollard, 2016; Edwards et al., 2019) [or subsections assumed to be independent \(Nias et al., 2019\)](#), a more sophisticated approach that preserves far more information is to decompose the spatial fields into orthogonal Principal Components (PCs) (Chang et al., 2016a, b; Holden et al., 2015; Sexton et al., 2012; Salter et al., 2018; Higdson et al., 2008). The decompositions are used as simplified representations of the original model ensemble in order to aid predicting [the](#) behaviour of computationally expensive models, and in some cases to restrict flexibility of the statistical model in parameter calibration so that the problem is computationally feasible and well-posed (Chang et al., 2016a, b). But the latter studies, which employ a formal probabilistic approach, still assume spacial and/or temporal independence at some point in the calibration. This independence assumption is not necessary if the weighting (likelihood) calculation is shifted from the spatio-temporal domain into that of principal component basis vectors, as proposed e.g. in Chang et al. (2014).

A further difficulty is the computational expense of Antarctic ice sheet models that have sufficient spatial resolution to resolve grounding line migration. This can be overcome by building an ‘emulator’, which is a statistical model of the response

of a physically-based computer model. Emulation allows a small ensemble of the original ice sheet model to be extended to a much larger number, ~~essentially by interpolation in the parameter space~~. This approach has ~~only~~ recently been applied in projections of the Antarctic ice sheet contribution to sea level rise (~~Edwards et al., 2019; Chang et al., 2016a, b~~) by interpolation in the input parameter space in general (Edwards et al., 2019; Chang et al., 2016a, b; Bulthuis et al., 2019) and melt forcing in particular (Levermann et al., 2014). Emulation becomes particularly important in model calibration, as this down-weights or rejects ensemble members and therefore reduces the effective ensemble size.

The aim of this study is to use a novel, practical, yet comprehensive calibration of the high-resolution Antarctic ice sheet model BISICLES to give smooth, refined probability functions for the dynamic sea level contribution from the Amundsen Sea Embayment for 50 years from the present day. We derive principal components of ice thickness change estimates with a singular value decomposition, thus exploiting more of the available information of satellite observations than previous studies. The statistical independence of those PCs aids the use of Bayesian ~~inference for probabilistic predictions~~ (probabilistic) inference. We use emulation of the ice sheet model to ensure dense sampling of the input space and therefore smooth probability density functions. Emulating the full spatial fields allows us to assess the probabilities not only of total mass loss (in mm Sea Level Equivalent, SLE) but also of the locations of grounding line retreat.

In Section 2 we describe the ice sheet model and satellite observation data, followed by our calibration approach in Section 3. In Section 4 we present the resulting probabilistic ice sheet ~~predictions~~ projections which are discussed in Section 5.

2 Model Ensemble and Observations

2.1 Ice sheet model ensemble

We use the ice sheet model ensemble published in Nias et al. (2016) using the adaptive mesh model BISICLES (Cornford et al., 2013) with equations from Schoof and Hindmarsh (2010). The mesh has a minimum spatial resolution of 0.25 km and evolves during the simulation. The model was run for the Amundsen Sea Embayment with constant climate forcing for 50 years with 284 different parameter configurations. ~~Three~~ Two uncertain inputs are varied categorically: two different bedrock elevation maps are used, as well as two different sliding law exponents. The first bedrock elevation map is Bedmap2, which is based on an extensive compilation of observations (Fretwell et al., 2013), while the second was modified by Nias et al. (2016) in order to reduce unrealistic model behaviour. The modifications are primarily local (<10 km) and include the removal of a topographic rise near the initial grounding line of Pine Island Glacier. The sliding law exponent defines the linearity of the basal ice velocity with basal traction, and values of 1 (linear) and 1/3 (power law) have been used. In addition, three scalar parameters were perturbed continuously, representing amplitude scalings of (1) the ocean-induced basal melting underneath ice shelves (i.e. the floating extensions of the ice streams), (2) the effective viscosity of the ice, determining the dynamic response to horizontal strain, and (3) the basal traction coefficient representing bedrock-ice interactions and local hydrology. The default values for these three parameters were determined for initialisation ~~of the model by Nias et al. (2016), using inversion from~~ by model inversion (Habermann et al., 2012; MacAyeal et al., 1995) of surface ice speeds (Rignot et al., 2011), and subsequently perturbed between half and double the default values in a Latin Hypercube design (Nias et al., 2016). We

use by (Nias et al., 2016). Different default basal traction coefficient fields have been found for each combination of bed topography and sliding law while the default viscosity field only differs between bed geometries (but not sliding laws). We use the normalized parameter ranges with halved, default and doubled scaling factors mapped to 0, 0.5 and 1, respectively. In addition, two further uncertain inputs are varied categorically: two different bedrock elevation maps are used, as well as two different sliding law exponents. The first bedrock elevation map is Bedmap2, which is based on an extensive compilation of observations (Fretwell et al., 2013), while the second was modified by Nias et al. (2016) in order to reduce unrealistic model behaviour. The modifications are primarily local (<

The ensemble covers a wide range of sea level rise contributions for the 50 year period with the most extreme members reaching -0.19 mm/year and 1.62 mm/year, respectively. About 10 km) and include the removal of a topographic rise near the initial grounding line of Pine Island Glacier. The sliding law exponent defines the linearity of the basal ice velocity with basal traction, and values of 1 (linear) and 1% of the ensemble shows an increasing volume above flotation (negative sea level contribution) and the central runs (0.5 for traction, viscosity and ocean melt parameters) contribute 0.27 mm/3 (power-law) are used. year (linear sliding) and 0.26 mm/year (nonlinear sliding). The average contributions are generally reasonably close to satellite observations (0.33 ± 0.05 mm/year from 2010-2013 (McMillan et al., 2014)) with 0.30 mm/year for linear sliding and modified bedrock, 0.37 mm/year for linear sliding and Bedmap-2, 0.38 mm/year for nonlinear sliding and modified bedrock and 0.51 mm/year for nonlinear sliding and Bedmap-2 (Nias et al., 2016).

For a full description of the model ensemble see Nias et al. (2016). For the calibration we allow for a short spin up phase of 3 years for the model to adjust to the perturbations and use the following 7 years as calibration period. Other calibration periods have been tested and show small impact on the results for calibrations in basis representation. We regrid the simulated surface elevation fields for the first 7 years this period to the same spatial resolution as the observations (10 km \times 10 km) by averaging.

We do use the whole model domain and a finer model resolution of 4 km \times 4 km for projections (after The sea level rise contribution at the end of the model period (50 years) because we are not restricted by the observational data characteristics. Besides this, the same methods (spatial decomposition and emulation, see below) are used for the projections (after 50 years) as for the calibration period. The spatial mask defining the catchment area is calculated directly on the model grid, using the same catchment area mask as in Nias et al. (2016) is used for sea level rise estimates.

2.2 Observations

We use a compilation of five satellite altimeter datasets of surface elevation changes from 1992-2015 by Konrad et al. (2017). The synthesis involves fitting local empirical models over spatial and temporal extents of up to 10 km and 5 years, respectively, as developed by McMillan et al. (2014). The satellite missions show high agreement, with a median mis-match of 0.09 m/year.

3 Theoretical basis and Calibration Model

Our In the following we propose a new ice sheet model calibration approach which will be tested in section 3.1 and compared to alternative approaches in section 3.2. This calibration approach consists of an emulation step and a calibration step. Emulation - statistical modelling of the ice sheet model - helps to overcome computational constraints and to refine probability density functions, while the subsequent calibration infers model parameter values which are likely to lead to good representations of the ice sheet. Both emulation and calibration take place in the basis representation of a Principal Component (PC) decomposition, in order to adequately represent spatial correlation and avoid unnecessary loss of information (e.g. by comparing total or mean model-observation differences). We build two spatial emulators: one represents the model response after the first 7 years of the simulation, which is used for calibration. The second construct a spatial emulator for the calibration period to represents the two dimensional model response in ice thickness change. A second, non-spatial emulator represents the response total sea level rise at the end of the 50 year simulation, and is used to make probabilistic predictions of total sea level contribution and spatial grounding line retreat simulations.

3.1 Principal Component Decomposition

Let $\mathbf{y}(\theta_i)$ be the m dimensional spatial ice sheet model model ice thickness change output for a parameter setting θ_i , where m is the number of spatial horizontal grid cells and the model ensemble has n members so that $\theta_1, \dots, \theta_n \in \Theta$, $\Theta \in \mathbb{R}^d$ being the parameter space which is $\theta_1, \dots, \theta_n = \Theta$, $\Theta \subset [0, 1]^d \subset \mathbb{R}^d$ being the whole set of input parameters, spanning in our case spanned by the $d = 5$ model input parameters dimensional model input space. The $m \times n$ matrix $\tilde{\mathbf{Y}}$ is the row-centered combined model output with the i .th column consisting of $\mathbf{y}(\theta_i)$ minus the mean of all ensemble members, $\bar{\mathbf{y}}$, and each row represents a single location. In the following we will assume $n < m$. A principal component decomposition is achieved by finding \mathbf{U} , \mathbf{S} and \mathbf{V} so that

$$\tilde{\mathbf{Y}} = \mathbf{U}\mathbf{S}\mathbf{V}^T \quad (1)$$

where the $n \times n$ $m \times n$ rectangular diagonal matrix \mathbf{S} contains the n positive singular values of $\tilde{\mathbf{Y}}$ and \mathbf{U} and \mathbf{V}^T are unitary. The rows of \mathbf{V}^T are the orthonormal eigenvectors of $\tilde{\mathbf{Y}}^T \tilde{\mathbf{Y}}$ and the columns of \mathbf{U} are the orthonormal eigenvectors of $\tilde{\mathbf{Y}} \tilde{\mathbf{Y}}^T$. In both cases the corresponding eigenvalues are given by $\text{diag}(\mathbf{S})^2$. By convention \mathbf{U} , \mathbf{S} and \mathbf{V}^T are arranged so that the values of $\text{diag}(\mathbf{S})$ are descending and we use $\mathbf{B} = \mathbf{U}\mathbf{S}$ as shorthand for the new basis and call the i .th column of \mathbf{B} the i .th principal component.

The fraction of ensemble variance represented by a principal component is proportional to its eigenvalue the corresponding eigenvalue of \mathbf{U} and typically there is a number $k < n$ for which the first k principal components represent the whole ensemble sufficiently well. We choose $k = 4$ for the emulator at the beginning of the model period and $k = 5$ for the second emulator at the end of the period so that in both cases $k = 5$ so that 90% of the model variance is captured (Appendix A)-Figure 1). The first k columns of \mathbf{U} are illustrated in Figure 1 which are related to the PCs (\mathbf{B}_i) by multiplication with the singular values.

$$\tilde{\mathbf{Y}} \approx \mathbf{U}'\mathbf{S}'\mathbf{V}'\tilde{\mathbf{Y}} \approx \mathbf{B}'\mathbf{V}'^T \quad (2)$$

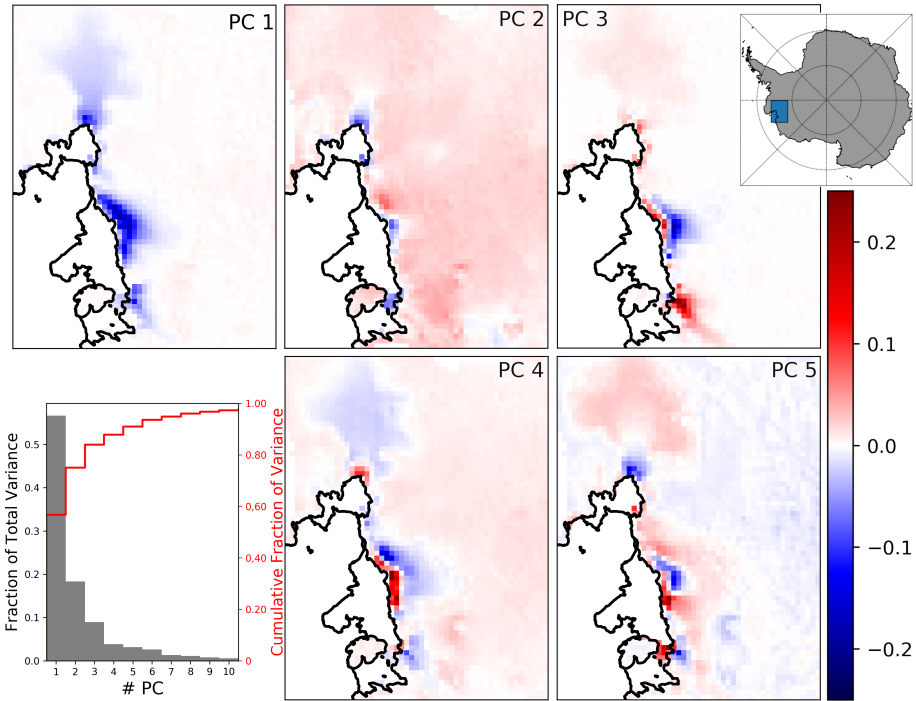


Figure 1. First four The first five normalized PCs, building an orthogonal basis. They represent the main modes of variation in the calibration period with unit length model ensemble

with \mathbf{U}' and \mathbf{V}' consisting of the first k columns of \mathbf{U} and \mathbf{V} , while \mathbf{S}' is the $k \times k$ upper left corner matrix of \mathbf{S} .

This decomposition reduces the dimensions from m grid cells to just k principal components. The PCs are by construction orthogonal to each other and can be treated as statistically independent.

3.2 Observations in basis representation

- 5 Spatial m dimensional observations $z_{(xy)}$ can be transformed to the basis representation by:

$$\hat{z} = \mathbf{U}'(\mathbf{B}'^T \mathbf{U}')^{-1} \mathbf{U}' \mathbf{B}'^T z_{(xy)} \quad (3)$$

for $z_{(xy)}$ on the same spatial grid as the model output $\mathbf{y}(\theta)$ which has the mean model output $\bar{\mathbf{y}}$ subtracted for consistency.

- We perform the transformation as in Equation 3 for all of the bi-yearly observations over a seven year period to get 14 different realizations of \hat{z} . Due to the smooth temporal behaviour of the ice sheet on these timescales we use the observations as repeated observations of the same point in time to specify \hat{z} as the mean and use the variance among the 14 realizations of \hat{z} to define the observational uncertainty in the calibration model (sec 3.4).

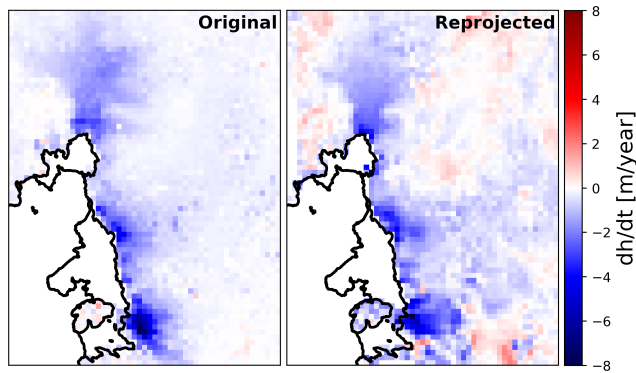


Figure 2. Left: Mean ~~observations~~observed ice thickness change. Right: ~~Observations~~Observed ice thickness change projected to first ~~4~~five PCs and reprojected to spatial field

Figure 2 shows that large parts of the observations can be represented by the first ~~4~~5 PCs from Fig. 1. It is only this part illustrated on the right of Fig. 2 which is used for calibration. The spatial variance of the difference between the reprojected and original fields is substantially smaller than from $z(xy)$ alone:

$$\frac{\text{VAR}(z(xy) - \mathbf{U}'((\mathbf{U}'^T \mathbf{U}')^{-1} \mathbf{U}'^T z(xy)))}{\text{VAR}(z(xy))} \frac{\text{VAR}(z(xy) - \mathbf{B}'((\mathbf{B}'^T \mathbf{B}')^{-1} \mathbf{B}'^T z(xy)))}{\text{VAR}(z(xy))} \approx 0.\underline{62}.\underline{58}$$

3.3 Emulation

- 5 For probabilistic ~~prediction-projections~~ we need to consider the probability density in the full, five-dimensional parameter space. This exploration can require very dense sampling of probabilities in the input space to ensure appropriate representation of all probable parameter combinations. This is especially the case if the calibration is favouring only small subsets of the original input space. In our case more than ~~half~~90% of the projection distribution would be based on just ~~six~~five BISICLES ensemble members. For computationally expensive models sufficient sampling can be achieved by statistical emulation, as laid
- 10 out in the following.

A row of \mathbf{V}'^T can be understood as indices of how much of a particular principal component is present in every ice sheet model simulation. Emulation is done by replacing the discrete number of ice sheet model simulations by continuous functions or statistical models. We use each row of ~~$\mathbf{S}'\mathbf{V}'^T$ in combination~~ \mathbf{V}'^T , combined with ~~Θ to train independent~~continuous statistical models, to train an independent statistical model where the mean of the random distribution at θ is

15 denoted $\omega_i(\theta)$. Here the training points are noise free as the emulator is representing a deterministic ice sheet model and therefore $\omega_i(\Theta) = [\mathbf{V}'^T]_i$ for principal components $i = 1, \dots, k$. Each of those ~~statistical~~ models can be used to interpolate (extrapolation should be avoided) between members of Θ to predict the ice sheet model behaviour and create surrogate ensemble members. ~~We call the aggregation of those statistical models an emulator.~~

We use Gaussian Process (GP) models, which are a common choice for their high level of flexibility and inherent emulation uncertainty representation (Kennedy and O’Hagan, 2001; O’Hagan, 2006; Higdon et al., 2008). [The random distribution of a Gaussian process model with noise free training data at a new set of input values \$\theta_*\$ is found by \(e.g. Rasmussen and Williams, 2006\)](#)

$$\Omega_{i*} = N(K(\theta_*, \Theta)K(\Theta, \Theta)^{-1}\omega_i(\Theta), K(\theta_*, \theta_*) - K(\theta_*, \Theta)K(\Theta, \Theta)^{-1}K(\Theta, \theta_*)) \quad (4)$$

where the values of $K(\Theta, \Theta)_{ij} = c(\theta_i, \theta_j)$ are derived from evaluations of the GP covariance function $c(\cdot, \cdot)$. Equivalent definitions are used for $K(\theta_*, \Theta)$, $K(\Theta, \theta_*)$ and $K(\theta_*, \theta_*)$, note that $K(\theta_*, \theta_*)$ is a 1×1 matrix if we emulate one new input set at a time. We use a Matern ($\frac{5}{2}$) type function for $c(\cdot, \cdot)$ which describes the covariance based on the distance between input parameters. Coefficients for $c(\cdot, \cdot)$ (also called hyper-parameters), including the correlation length scale, are optimized on the marginal likelihood of $\omega(\Theta)$ given the GP. We refer to Rasmussen and Williams (2006) for an in-depth discussion and tutorial of Gaussian Process Emulators. ~~The emulator can be described as a joint Gaussian distribution:-~~

$$\Omega = N(\omega(\theta), \Sigma_\omega(\theta))$$

where Σ_ω is the $k \times k$ emulator co-variance matrix and ω the emulator mean vector for any given θ . Here Σ_ω is diagonal due to the statistical independence of the principal components. ~~The diagonal values of Σ_ω are derived from the corresponding Gaussian Process models and are dependant on the distance between the new θ , for which the emulator is evaluated, and the training points from the ice sheet model. The nature of this distance dependency is defined by the Gaussian Process covariance function which we define as Matern ($\frac{5}{2}$) type with length scales optimized on the marginal likelihood we can combine the k GPs to:~~

$$\Omega = N(\omega(\theta), \Sigma_\omega(\theta)) \quad (5)$$

The combined Ω is in the following called emulator and $\omega(\theta)$ as well as the entries of the diagonal matrix $\Sigma_\omega(\theta)$ follow from equation 4. We use the python module GPy for training (GPyRegression()) and marginal likelihood optimization (optimize_restarts()). In total we generate more than 119 000 emulated ensemble members. Emulator estimates of ice sheet model values in a leave-one-out cross-validation scheme are very precise with squared correlation coefficients for both emulators of $R^2 > 0.993$ (Appendix A $R^2 > 0.988$ (See supplement for more information)).

3.4 Calibration Model

Given the emulator in basis representation, a calibration can be performed either after re-projecting the emulator output back to the original spatial field (Chang et al., 2016a; Salter et al., 2018, e.g.) (e.g. Chang et al., 2016a; Salter et al., 2018) or in the basis representation itself (Higdon et al., 2008, e.g.) (e.g. Higdon et al., 2008; Chang et al., 2014). Here we will ~~base probability statements focus~~ on the PC basis representation.

We assume the existence of a parameter configuration θ^* within the bounds of Θ which leads to an optimal model representation of the real world. To infer the probability of any θ to be θ^* we rely on the existence of observables, i.e. model quantities z for which corresponding measurements \hat{z} are available. We follow Bayes' theorem to update prior (uninformed) expectations about the optimal parameter configuration with the observations to find posterior (updated) estimates. The posterior probability of θ being the optimal θ^* given the observations is:

$$\pi(\theta|z = \hat{z}) \propto L(z = \hat{z}|\theta) \times \pi(\theta) \quad (6)$$

where $L(z = \hat{z}|\theta)$ is the likelihood of the observables to be as they have been observed under the condition that θ is θ^* , and $\pi(\theta)$ is the prior (uninformed) probability that $\theta = \theta^*$. Following Nias et al. (2016) we choose uniform prior distributions in the scaled parameter range $[0,1]$ (see also section 2 and eqEq. 11 in Nias et al. (2016)). ~~We relate the observables~~ The emulator output is related to the real state of the ice sheets in basis representation, γ , by ~~the model discrepancy ε :~~

$$\gamma = \omega(\theta^*) + (\mathbf{U}'^T \mathbf{U}')^{-1} \mathbf{U}'^T \varepsilon \quad (7)$$

We assume the model discrepancy to be multivariate Gaussian distributed with zero mean; $\varepsilon = N(0, \Sigma_\varepsilon)$. The observables are in turn related to γ by:

$$z = \gamma + (\mathbf{B}'^T \mathbf{B}')^{-1} \mathbf{B}'^T e \quad (8)$$

where e is the spatial observational error and the transformation ~~$(\mathbf{U}'^T \mathbf{U}')^{-1} \mathbf{U}'^T$ follows from equ 3. The emulator output is related to γ by the model discrepancy ε :~~

$$\gamma = \omega(\theta^*) + \varepsilon$$

$(\mathbf{B}'^T \mathbf{B}')^{-1} \mathbf{B}'^T$ follows from Eq. 3.

We simplify the probabilistic inference by assuming the ~~observational error e ,~~ model error/discrepancy ε ~~and,~~ the model parameter values ~~Ω Θ and observational error e~~ to be mutually statistically independent ~~with $\varepsilon = N(0, \Sigma_\varepsilon)$. We further assume the observational error and e~~ to be spatially identically distributed with variance σ_e^2 , so that

$$(\mathbf{U}' (\mathbf{B}'^T \mathbf{U}')^{-1} \mathbf{U}' \mathbf{B}')^{-1} \mathbf{B}'^T e = N(0, \sigma_e^2 (\mathbf{U}' (\mathbf{B}'^T \mathbf{U}')^{-1} \mathbf{B}')^{-1}) \quad (9)$$

The $k \times k$ matrix ~~$(\mathbf{U}'^T \mathbf{U}')^{-1} (\mathbf{B}'^T \mathbf{B}')^{-1}$~~ is diagonal with the element-wise inverse of $diag(\mathbf{S}')_i^2$ as diagonal values. We estimate σ_e^2 from the variance among the 14 observational periods for the first principal component constituting \hat{z}_1 , i.e.

$$\sigma_e^2 = VAR(\hat{z}_1) \cdot diag(\mathbf{S}')_1^2 \quad (10)$$

Note that the existence of γ is an abstract concept, implying that it is only because of an error ε that we cannot create a numerical model which is equivalent to reality. However abstract, it is a useful, hence common statistical concept allowing us to structure expectations of model and observational limitations (Kennedy and O'Hagan, 2001). Neglecting model

~~uncertainty~~discrepancy, whether explicitly by setting $\varepsilon = 0$, or implicitly, would imply that ~~the-an~~ ice sheet model can make exact predictions of the future once the right parameter values are found. This expectation is hard to justify considering the assumptions which are made for the development of ice sheet models, including sub-resolution processes. Neglecting model discrepancy typically results in overconfidence and potentially biased results.

5 ~~It follows from equations 5, 8, 7 and 9 that~~

$$L(\mathbf{z} = \hat{\mathbf{z}}|\boldsymbol{\theta}) \propto \exp \left[-\frac{1}{2}(\boldsymbol{\omega}(\boldsymbol{\theta}) - \hat{\mathbf{z}})^T \boldsymbol{\Sigma}_T^{-1}(\boldsymbol{\omega}(\boldsymbol{\theta}) - \hat{\mathbf{z}}) \right]$$

~~with $\boldsymbol{\Sigma}_T = \sigma_\varepsilon^2(\mathbf{U}'^T \mathbf{U}')^{-1} + \boldsymbol{\Sigma}_\varepsilon + \boldsymbol{\Sigma}_\omega$.~~

~~The inclusion of systematic model uncertainties can~~ At the same time can the inclusion of model discrepancy lead to identifiability issues where the model signal cannot be distinguished from imposed systematic model ~~uncertainty (discrepancy) error~~.

10 To overcome such issues, constraints on the, e.g. spatial shape, of the discrepancy ~~can be~~ are used (Kennedy and O'Hagan, 2001; Higdon et al., 2008). An inherent problem with representing discrepancy is that its amplitude and spatial shape are in general unknown. If the discrepancy were well understood the model itself or its output could be easily corrected. Even if experts can specify regions or patterns which are likely to show inconsistent behaviour, it cannot be assumed that these regions or patterns are the only possible forms of discrepancy. If its representation is too flexible it can however become numerically
15 impossible in the calibration step to differentiate between discrepancy and model behaviour.

For these reasons we choose a rather heuristic method which considers the impact of discrepancy on the calibration directly and independently for each PC. Therefore $\boldsymbol{\Sigma}_\varepsilon$ is diagonal with $diag(\boldsymbol{\Sigma}_\varepsilon) = (\sigma_{\varepsilon_1}^2, \dots, \sigma_{\varepsilon_k}^2)^T$. ~~A common rule of thumb is~~ The 'three sigma rule' states that at least 95% of ~~a probability distribution lies~~ continuous unimodal density functions with finite variance lie within three standard deviations from the mean (Pukelsheim, 1994). For the i .th PC we ~~find $\sigma_{\varepsilon_i}^2$ therefore find σ_{i95}^2~~
20 so that 95% of the observational distribution $N(\hat{z}_i, \sigma_{\varepsilon_i}^2)$ lies within ~~$3\sigma_{\varepsilon_i}$~~ $3\sigma_{i95}$ from the mean of $\boldsymbol{\omega}(\boldsymbol{\Theta})_i$, i.e. across the n ensemble members. We ~~further note that we do not know the optimal model setup better than we know the real state of the ice sheet and set the minimum discrepancy to the observational uncertainty. Hence $\sigma_{\varepsilon_i}^2 = MAX(\sigma_{i95}^2, \sigma_{\varepsilon_i}^2)$.~~

We thereby force the observations to fulfill the 'three-sigma rule' by considering them as part of the model distribution $\boldsymbol{\omega}(\boldsymbol{\Theta})_i$ while avoiding over confidence in cases where observations and model runs coincide.

25 3.4.1 History matching

Probabilistic calibrations search for the best input parameters, but stand-alone probabilistic calibrations cannot guarantee that those are also 'good' input parameters in an absolute sense. While 'good' is subjective, it is possible to define and rule out implausible input parameters. The Implausibility parameter is commonly defined as (e.g. Salter et al., 2018):

$$\mathcal{I}(\boldsymbol{\theta}) = (\boldsymbol{\omega}(\boldsymbol{\theta}) - \hat{\mathbf{z}})^T \boldsymbol{\Sigma}_T^{-1}(\boldsymbol{\omega}(\boldsymbol{\theta}) - \hat{\mathbf{z}}) \tag{11}$$

30 with $\boldsymbol{\Sigma}_T = \sigma_\varepsilon^2(\mathbf{B}'^T \mathbf{B}')^{-1} + \boldsymbol{\Sigma}_\varepsilon + \boldsymbol{\Sigma}_\omega$. A threshold on $\mathcal{I}(\boldsymbol{\theta})$ can be found using the 95% interval of a chi-squared distribution with $k = 5$ degrees of freedom. Therefore we rule out all $\boldsymbol{\theta}$ with $\mathcal{I}(\boldsymbol{\theta}) > 11$. By adding this test, called history matching, we

ensure that only those input parameters are used for a probabilistic calibration which are reasonably close to the observations. In the worst case the whole input space could be ruled out, forcing the practitioner to reconsider the calibration approach and uncertainty estimates. Here about 1.4% of the parameter space cannot be ruled out.

3.4.2 Probabilistic Calibration

5 For all θ which have not been ruled out, the likelihood $L(z = \hat{z}|\theta)$ follows from equations 5, 8, 7 and 9:

$$L(z = \hat{z}|\theta) \propto \exp \left[-\frac{1}{2}(\omega(\theta) - \hat{z})^T \Sigma_T^{-1} (\omega(\theta) - \hat{z}) \right] \quad (12)$$

The calibration distribution in Equation 6 can be evaluated using Eq. 12 with a trained emulator (Eq. 54), observational (Eq. 10) and model ~~uncertainties~~-discrepancy (above) and the prior parameter distributions $\pi(\theta)$ set by expert judgment.

4 Results

10 3.1 Calibration model test

In this section we test our calibration approach on synthetic observations to see whether our method is capable of finding known-correct parameter values. We select one member of the BISICLES model ensemble at a time and add 14 different realizations of noise to it. The noise is added to see how the calibration performs if the observations cannot be fully represented by the ice sheet model.

15 3.2 Parameter calibration

We use spatially independent, zero-mean, normally distributed, random noise with variance equal to the local variance from the 14 periods of satellite observations. This way the variance incorporates dynamic changes (acceleration/deceleration of the ice thickness change) and technical errors (e.g. measurement and sampling errors). For each selected model run we generate 14 noise fields and add them to the single model ice thickness change field. These 14 realizations are used in exactly the same way as described before for the 14 periods of satellite observations.

Likelihood of different model inputs (evaluations of Equation 12). Upper right panels show likelihood values marginalized to pairs of parameters, normalized to the respective maximum for clarity. Lower left panel shows likelihood values marginalized to individual parameters for the three scalar parameters (line plots), and sliding law and bedrock topography map (text and quotation within), normalized to an integral of one in the style of Probability Density Functions. For Figure 3 the model run with central parameter values ($= 0.5$) for basal traction, viscosity and ocean melt scaling factors, nonlinear sliding and modified bedrock has been selected, as indicated by black circles. This parameter set has been selected as it highlights the limitations of the calibration, but the results of many other synthetic model tests are shown in the supplement.

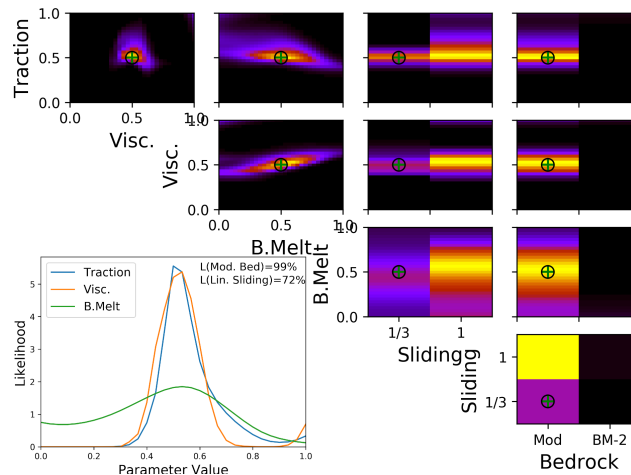


Figure 3. Mean sea level contributions at end Likelihood of 50-year model period as in Fig. 5. For each parameter combination (upper right panels) or single parameter value combinations of synthetic test case (line evaluations of Equation 12). Upper right panels show likelihood values marginalized to pairs of parameters, normalized to the mean sea level contributions across all other respective maximum for clarity. Lower left panel shows likelihood values marginalized to individual parameters is calculated using for the prior distributions three scalar parameters (line plots), and sliding law and bedrock topography map (text and quotation within), normalized to an integral of one, consistent with Probability Density Functions. The central values for traction, viscosity and ocean melt as well as nonlinear sliding and modified bedrock are used. The parameter values are also shown by the black circles, while the values of the set of parameters with highest likelihood are shown by green crosses (equal weights)

Figure 5-3 illustrates which parts of the model input space are most successful in reproducing the satellite synthetic observations of surface elevation changes during the initial part of the simulation calibration period. For visualisation we collapse the five dimensional space onto each combination of two parameters and show how they interact. For a likely (yellow) area in Fig. 5-3 it is not possible to see directly what values the other three parameters have, but very unlikely (black) areas indicate that no combination of the remaining parameter values results in a good model configuration.

The calibration has the strongest effect on selecting the bedrock topography map and sliding law exponent. We find that the modified bedrock from Nias et al. (2016) produces much more realistic surface elevation changes than the original Bedmap2 topography (Fig. 5), and the linear sliding law is more successful than the non-linear ($m = \frac{1}{3}$). We find the most likely fields of basal traction and velocity are the default values (i.e. scaling factor of 0.5) inferred by (Nias et al., 2016) from inversion from surface ice speeds; this confirmation through two independent datasets suggests good model consistency. The sub-shelf melting field is constrained the least (all values of the scaling factor are similarly likely), probably due to the short calibration period, but higher melt rates are found to be slightly more likely than lower rates. Nias et al. (2016) find the model sensitivity to ocean melt to be considerably smaller than to viscosity and traction, in particular for the large Thwaites Glacier. The parameter combination with the highest likelihood has values of 0.43 for basal traction, 0.53 for viscosity. As can be seen from Figure 3, marginal likelihoods of our calibration approach can favour linear sliding even if the synthetic observations use nonlinear

sliding. In addition, the ocean melt parameter is often weakly constrained or, as in this case, biased towards small melt factors. In contrast, the basal traction coefficient and viscosity scaling factors have a strong mode at, or close to, the correct value of 0.5 and the correct bedrock map can always be identified (Figure 3 and supplement). Different values of basal traction and viscosity have been tested in combination with both bedrock maps and show similar performance (see supplement). The fact that the parameter setup used for the test is attributed the maximal likelihood (green cross on top of black circle) supports our confidence in the implementation as the real parameter set is identified correctly as best fit. Relative ambiguity with respect to sliding law and ocean melt overrules the weak constraints on these parameters in the marginalized likelihoods. The higher total likelihood of linear sliding can be traced back to a higher density of central ensemble members for linear sliding. Nonlinear sliding produces more extreme ice sheet simulations as fast simulations will have reduced (compared to linear sliding) basal drag and become even faster (and vice versa for slow simulations). The frequency distribution of total sea level contribution and basis representation are therefore wider for nonlinear sliding (supplement). The relative density of ensemble members around the mode of the frequency distribution can, as for this test case, cause a smaller marginal likelihood for nonlinear sliding compared to linear sliding (28% to 72%).

But why is the signal of sliding law and ocean melt not strong enough to adequately constrain the calibration, and even though both parameters are known (Arthern and Williams, 2017; Joughin et al., 2019) to have a strong impact on model simulations? This is likely related to the delayed impact of those parameters compared to the others. The perturbation of ocean melt from the start of the model period has to significantly change the ice shelf thickness before the ice dynamics upstream are affected. The fields of basal traction coefficient are adjusted to the sliding law by the inversion of surface ice velocities so that the initial basal drag τ_b is approximately the same for both sliding laws with:

$$\tau_b = C_m(x, y) \cdot |v(x, y, t)|^{m-1} \cdot v(x, y, t) \quad (13)$$

where $C_m(x, y)$ is the spatial basal traction coefficient for sliding law exponent m ($m = 1$ for linear, $m = 1/3$ for nonlinear sliding) and $v(x, y, t)$ being the basal ice velocity. As $C_m(x, y)$ compensates for $|v(x, y, t)|^{m-1}$ at the beginning of the model period, it is only after the ice velocities change that the sliding law has any impact on the simulations. A change in bedrock, basal traction or viscosity have, however, a much more immediate effect on the ice dynamics and are therefore expected to dominate the calibration on short time scales.

From this test we conclude that basal sliding law and ocean melt scaling cannot be inferred from this calibration approach. We will therefore only calibrate the bedrock as well as basal traction and viscosity scaling factors. Several studies used the observed dynamical changes of parts of the ASE to test different sliding laws. Gillet-Chaulet et al. (2016) find a better fit to evolving changes of Pine Island Glacier surface velocities for smaller m , reaching a minimum of the cost function from around $m=1$ (maximum) for ocean melt factor, with a linear sliding law /5 and smaller. This is supported by Joughin et al. (2019) who find $m=1/8$ to capture the PIG speed up from 2002 to 2017 very well, matched only by a regularized Coulomb (Schoof-) sliding law. It further is understood, that parts of the ASE bed consist of sediment-free, bare rocks for which a linear Weertman sliding law is not appropriate (Joughin et al., 2009). We therefore select nonlinear sliding by expert judgment and use a uniform prior for the ocean melt scaling.

3.2 Comparison with other calibration approaches

To put the likelihood distribution from Figure 3 into context, we try two other methodical choices. First we calibrate in the spatial domain after re-projecting from the emulator results.

$$\mathbf{y}'(\boldsymbol{\theta}) = \mathbf{B}'\boldsymbol{\omega}(\boldsymbol{\theta}) \quad (14)$$

- 5 where $\mathbf{y}'(\boldsymbol{\theta}_i)$ are the re-projected ice sheet model results after truncation for parameter setup $\boldsymbol{\theta}$. We set the model discrepancy to twice the observational uncertainty σ_e^2 so that the re-projected likelihood $L_{(xy)}$ simplifies to:

$$L_{(xy)}(\mathbf{z}_{(xy)}|\boldsymbol{\theta}) \propto \prod_{i=1}^m \exp\left[-\frac{1}{2} \frac{(y'(\boldsymbol{\theta})_i - z_{(xy)i})^2}{3\sigma_e^2}\right] \quad (15)$$

Another approach is to use the net yearly sea level contribution from the observations $SLC(\mathbf{z}_{(xy)})$ and model $SLC(\mathbf{y}'(\boldsymbol{\theta}_i))$ for calibration, as done in e.g. Ritz et al. (2015).

$$10 \quad L_{SLC}(\mathbf{z}_{(xy)}|\boldsymbol{\theta}) \propto \exp\left[-\frac{1}{2} \frac{(SLC(\mathbf{y}'(\boldsymbol{\theta})) - SLC(\mathbf{z}_{(xy)}))^2}{3\sigma_{SLC}^2}\right] \quad (16)$$

Again, we set the model discrepancy to twice the observational uncertainty which we find from the variance of the yearly sea level contributions for the 14 bi-yearly satellite intervals. $\sigma_{SLC}^2 = VAR(SLC(\mathbf{z}_{(xy)})) = 0.035^2 \left[\frac{mmSLE^2}{year^2}\right]$.

- The calibration in (x,y) representation (Figure 4a) behaves similarly to the basis representation (Figure 3) in that sliding law exponent and, to a lesser degree, basal melt are weakly constrained while the confidence in the correctly identified traction and viscosity values is even higher. Using only the net sea level rise contribution constrains the parameters weakly; it shares the limitations of not constraining the ocean melt and favouring linear sliding but in addition, a wide range of traction-viscosity combinations perform equally well and there is no constraint on bedrock (Figure 4b). Furthermore, the model run used as synthetic observations is not identified as the most likely setup in Figure 4b. This demonstrates the value of the extra information - and stronger parameter constraints - provided by the use of two-dimensional observations.

20 4 Results

Following the synthetic model test, we now calibrate traction, viscosity and bedrock with the satellite data.

- The calibration finds that the modified bedrock from Nias et al. (2016) produces much more realistic surface elevation changes than the original Bedmap2 topography (Fig. 5a). The weighted average of basal traction and velocity parameters are 0.47 and the modified bedrock topography. However, for probabilistic predictions we do not focus on just this one parameter configuration but use the whole input space weighted by probability. 0.45, respectively, which is slightly smaller the default values (0.5). This amounts to a 3.5% and 7.2% reduction in amplitude compared to the optimized fields from by (Nias et al., 2016).

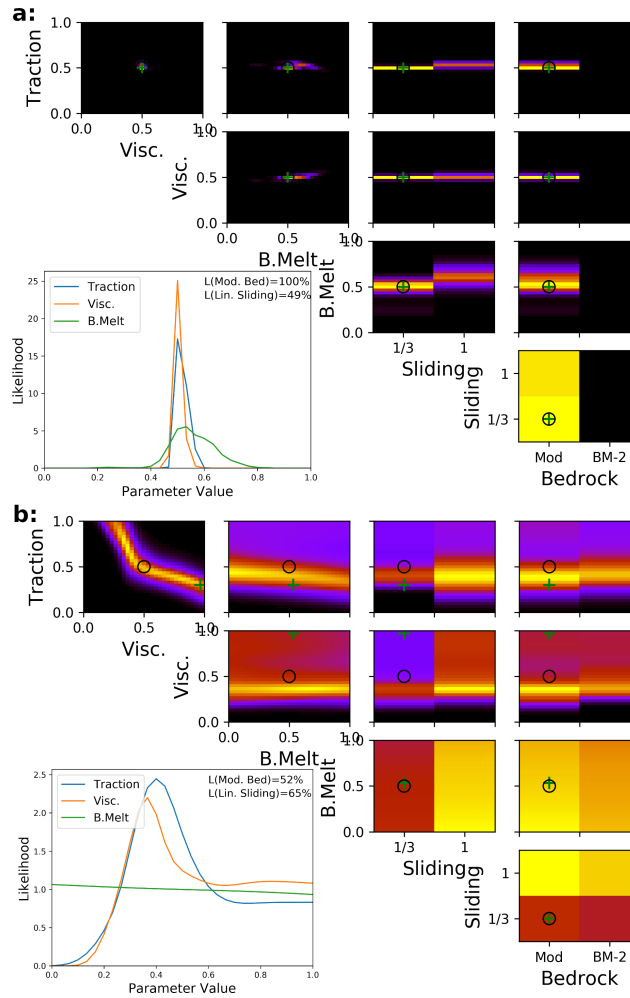


Figure 4. Likelihood of parameter combinations of synthetic test case for reprojected emulator estimates (top, a; Equation 15) and sea level rise contribution calibration (bottom, b; Equation 16). Upper right panels show likelihood values marginalized to pairs of parameters, normalized to the respective maximum for clarity. Lower left panel shows likelihood values marginalized to individual parameters for the three scalar parameters (line plots), and sliding law and bedrock topography map (text and quotation within), normalized to an integral of one, consistent with Probability Density Functions. The central values for traction, viscosity and ocean melt as well as nonlinear sliding and modified bedrock are used. The parameter values are also shown by the black circles, while the values of the set of parameters with highest likelihood are shown by green crosses.

4.1 Sea Level Contribution Projection

We use the calibration [in basis representation \(likelihood shown in Fig. 5a\)](#) as well as the reprojected (x,y) and SLC based calibrations to update the [predictions-projections](#) of sea level contribution and grounding line retreat after 50 years. ~~Total sea level contribution from the Amundsen Sea Embayment after 50 years. The full (shaded) and probability weighted (intense~~

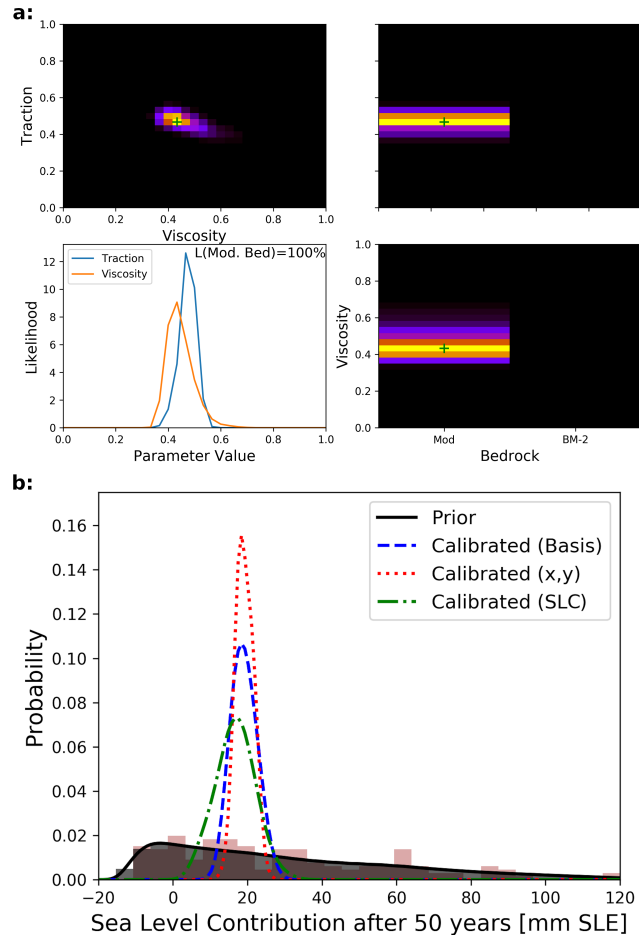


Figure 5. a: Likelihood of parameter combinations in basis representation from satellite observations (evaluations of Equation 12). Upper right panels show likelihood values marginalized to pairs of parameters, normalized to the respective maximum for clarity. Lower left panel shows likelihood values marginalized to individual parameters for the two scalar parameters (line plots) and bedrock topography map (text and quotation within), normalized to an integral of one in the style of Probability Density Functions. Values of the set of parameters with highest likelihood are shown by green crosses. b: Projected sea level rise contributions at the end of model period for uncalibrated BISICLES runs (brown shades), uncalibrated emulator calls (Grey shade) and different calibration approaches (colored lines).

colors) emulated ensemble distributions are shown. in Figure 5b. As can be seen from the Grey and Brown shaded histograms in Figure 5b (emulated and original BISICLES ensemble) the emulation helps to overcome challenges of limited sample size.

The calibrated prediction distribution is centred around the mode of the uncalibrated distribution, but sharper (i.e. reduced uncertainty) and much more symmetric (Fig. ?? and Table 1). This is most striking at the upper end of the distribution: the 95th percentile decreases from 78.2 to 23.3 mm SLE. We can also essentially rule out (<5%) negative sea level contributions. The tail is mostly rejected by downweighting of model simulations in which both the basal traction and basal viscosity scaling

5

Table 1. Total sea level contribution after 50 years in mm SLE: (weighted) mean, most likely model-configuration-contribution and percentiles; with and without calibration/calibrations.

	Mean	Mode	$\max(L(z=\hat{z} \theta))$ -5%	25%	50%	75%	95%
<u>Prior year 50-25.6</u> <u>Prior</u>	<u>9.6-30.6</u>	<u>—-3.3</u>	<u>-5.9-8.4</u>	<u>6.8-4.2</u>	<u>20.2-23.1</u>	<u>37.9-51.3</u>	<u>78.2-94.5</u>
<u>Posterior year 50-basis</u>	<u>11.4-19.1</u>	<u>10.4-18.4</u>	<u>13.9</u>	<u>16.7</u>	<u>18.9</u>	<u>21.4</u>	<u>24.8</u>
<u>Posterior (x,y)</u>	19.2	<u>0.6-18.4</u>	<u>6.3-16.7</u>	<u>11-17.7</u>	<u>16.1-18.6</u>	<u>23.3-21.1</u>	<u>22.2</u>
<u>Posterior SLC</u>	<u>16.8</u>	<u>17.5</u>	<u>7.7</u>	<u>13.2</u>	<u>16.8</u>	<u>20.3</u>	<u>25.6</u>

factors are small, because these give unrealistically large surface elevation decreases (compare Fig. 5 and ??). The second most important factor is the preference for the linear sliding law; again, three calibration approaches are consistent (large overlap) while using the reprojection approach leads to the power-law tends to give greater ice thinning rates than linear sliding. Bedrock topography is less important than the sliding law but the use of the modified bedrock in the uncalibrated distribution reduced the mean sea level contribution nevertheless by about 20% (Fig. ??; Nias et al., 2016).

The most narrow SLC distribution (Figure 5b), as was indicated by the findings of Section 3.2. Calibration on the total sea level contribution from the best (maximum likelihood) ensemble member over the 50 year period is 19.2 mm, notably higher than the distribution mean, mode and median (-10-11 mm SLE). This ensemble member has the highest possible value for the ocean melt factor (1). This causes more ensemble members to have smaller rather than larger sea level contributions hence influencing the mean and median in this direction. leads to a wider distribution with the lower bound of projections (5 %-ile) being more than 6 mm SLE smaller than for the two other approaches. All of them strongly reduce projection uncertainties compared to the uncalibrated prior distribution (Figure 5b and Table 1)

4.1 Grounding line retreat probabilities

Figure ?? shows the probabilities of regions to become ungrounded for the prior (uncalibrated) and posterior (calibrated) distributions. The area potentially affected by a grounding line retreat is considerably smaller after calibration, which is consistent with the reduced upper tail of total sea level contribution in Fig. ?. In other words, substantial grounding line retreat is simulated with low basal traction and viscosity, or a power law basal sliding law, but these are found to be much less consistent with recent surface elevation observations. However, all glaciers (Pine Island, Thwaites and Smith/Pope) retreat to some degree, and the farthest retreat is ≈ 28 km for Smith Glacier.

Probability density estimates of grounding line retreat after 50 years, uncalibrated (left) and calibrated (right). Labeled glaciers include Pine Island (PI) and Thwaites (TH). Initially ungrounded areas are masked in gray to highlight retreat, black lines show estimates of the grounding line and ice cliffs (MODIS Mosaic of Antarctica 2009 (Scambos et al., 2007)).

5 Discussion

In general, previous Antarctic ice sheet model uncertainty studies have either focused on parameter inference (Chang et al., 2016a, b; Pollard et al., 2016), or made projections that are not calibrated with observations (Nias et al., 2016; Schlegel et al., 2018; Bulthuis et al., 2019; Cornford et al., 2015), with the remaining probabilistic calibrated projections being based on simple
5 (fast) models using highly aggregated observations and some relying heavily on expert judgment (Ruckert et al., 2017; Ritz et al., 2015; Little et al., 2013; Levermann et al., 2014; DeConto and Pollard, 2016; Edwards et al., 2019). Here we perform statistically-founded parameter inference using spatial observations to calibrate high resolution (\sim grounding line resolving)
~~model predictions of both sea level contribution and grounding line retreat~~ ice sheet model projections.

~~Our Bayesian calibration of the sliding law with surface elevation changes is consistent with the Bayesian calibration with
10 ASE mass loss of (Ritz et al., 2015), who find that the linear sliding law is more likely to produce mass loss rates consistent with observed than nonlinear and plastic laws. However, Joughin et al. (2009) find a linear law underestimates sensitivity to basal traction.~~

The modified bedrock removes a topographic rise near the initial grounding line of Pine Island Glacier which could be caused by erroneous observations (Rignot et al., 2014). This rise, if present, would have a stabilizing effect on the grounding
15 line and simulations without it can result in more than twice the ~~predicted~~ sea level contribution from Pine Island Glacier for some sliding laws (Nias et al., 2018). Here we find the modified bedrock topography to produce a spatial response far more consistent with observed surface elevation changes than for the original Bedmap2 bedrock (Fig. 5) ~~while a calibration with total mass loss alone cannot distinguish between the two (see Figure 2 of Nias et al. (2016)).~~ ~~Calibrated predictions for this region based on Bedmap2 are likely to either be compensating the overly stabilising bedrock with underestimated viscosity and/or traction coefficients, or underestimating the sea level contribution altogether. Note that the a).~~ The modified bedrock
20 has been derived by reducing clearly unrealistic behaviour of the same ice sheet model, a better calibration performance ~~is~~ was therefore to be expected. However, no satellite observations have been used for the bedrock modification, nor has there ~~a~~ been a quantitative probabilistic assessment.

The non-spatial calibration on total sea level contribution alone cannot distinguish between the two bedrocks (Figure 4b).
25 Projections for this region based on Bedmap2, calibrated on the SLC are likely to either be compensating the overly stabilising bedrock with underestimated viscosity and/or traction coefficients, or underestimating the sea level contribution altogether. In addition to the unconstrained bedrock, the SLC calibration permits a wide range of traction and viscosity coefficients, including values far from the correct test values (Figure 4b). This shows that the SLC calibration permits more model runs which are right for the wrong reasons; they have approximately the right sea level rise contribution in the calibration period but can still
30 be poor representations of the current state of the ice sheet.

The extremely small area of likely input parameters for the reprojected (x,y) calibration (Figure 4a and Supplement) could indicate overconfidence in the retrieved parameter values, but could also mean that the available information is exploited more efficiently. Using subsections of the calibration period has a small impact on basis and SLC calibration. However, for one of the sub-periods with reprojected calibration the probability interval does not overlap with the results of the whole 7 year

calibration period (Table 1 in the Supplement). Since the sub-period is part of the 7 year period we would expect the results to be non-contradictory, indicating that the probability intervals are too narrow and hence the approach, as implemented here, being overconfident. The different ways of handling model discrepancy influence width of the probability intervals.

5 Satellite-based estimates for the Amundsen Sea Embayment of 0.33 mm SLE per year (McMillan et al., 2014) from 2010-2013 are higher than the mode of our sea level contribution distribution of about 0.21 mm SLE per year but similar to the 75th percentile.

Even though the most extreme retreat scenarios are essentially ruled out by the calibration The average sea level contribution from the observations used here is 0.36 mm SLE per year, consistent with estimates from McMillan et al. (2014) of 0.33 ± 0.05 mm SLE per year for the Amundsen Sea Embayment from 2010-2013. Calibrated rates in the beginning of the model period are very similar (0.335, we see several locations with high probability to become ungrounded. Most prominent is the retreat of Smith Glacier (Fig. ??). Previous studies have shown how far the grounding line could retreat for different model ensembles and climate scenarios (Nias et al., 2016; Bulthuis et al., 2019; Ritz et al., 2015), but only (Ritz et al., 2015) provide calibrated probabilistic estimates to compare with here. The resolution of their model is far lower (15 km), but the pattern approximately corresponds to their 95% probability contour by 2100 for Pine Island and Thwaites Glacier. Comparison with present day observations of grounding line retreat for Thwaites Glacier (for 2018; Milillo et al., 2019) and the Pope/Smith/Kohler region (for 2014; Scheuchl et al., 2016) show good agreement of the locations of retreat (e.g. far retreat at Smith with minimal retreat of Kohler glacier). However, large parts of the retreat predicted in this study for 0.327 and 0.363 mm SLE for basis, (x,y) and SLC, respectively). For (x,y) and basis calibration the rates increase over the 50 year period (starting somewhere between year 2000 and 2010) has been reached already. There are two possible explanations for this: the grounding line has reached a new stable location supported by topographic features (which are visible in Milillo et al. (2019) and Scheuchl et al. (2016)) while the rate of mass loss reduces for the SLC calibration (50 year average SLC rates: 0.382, where it will remain for the next decades, or else we underestimate the rate of retreat and with it potentially the rate of mass loss 0.384 and 0.336 mm SLE per year for basis, (x,y) and SLC., respectively). The fact that the SLC calibration starts with the largest rates of sea level contribution but is the only approach seeing a reduction in those rates, in combination with the above mentioned suspicion of it allowing unrealistic setups, raises questions about how reliable calibrations on total sea level contribution alone are.

The ice sheet model data used here is not based on a specific climate scenario but instead projects the state of the ice sheet under current conditions into the future (with imposed perturbations). Holland et al. (2019) suggest a link between anthropogenic greenhouse gas emissions and increased upwelling of warm circumpolar deep water, facilitating melt at the base of Amundsen sea ice shelves. This would imply a positive, climate scenario dependent trend of ocean melt for the model period, superimposed by strong decadal variability (Holland et al., 2019; Jenkins et al., 2016). Warmer ocean and air temperatures would enhance melt and accelerate the dynamic response. Neither do the used simulations carry the countervailing predicted increase of surface accumulation in a warmer climate (Lenaerts et al., 2016). Edwards et al. (2019); Golledege et al. (2019) found Edwards et al. (2019) and Golledege et al. (2019) find that the Antarctic ice sheet response to very different greenhouse gas emissions scenarios starts to diverge from around 2060-2070, indicating that scenario while Yu et al. (2018) find ocean

melt to have a negligible impact for the first 30 years for their simulations of Thwaites glacier. Combined, this is indicating that climate scenarios would have a small net impact on our 50-year projections.

~~The theoretical basis for most of the methodology used here has been laid out in Higdon et al. (2008), including the principal component decomposition, emulation and model calibration in the PC space. This calibration in basis (PC) representation has been adapted and tested for general circulation (climate) and ocean models Sexton et al. (2012); Chang et al. (2014); Salter et al. (2018); Sa-~~
5 ~~-By combining this approach with a simple but robust discrepancy representation, we attempt to bridge the gap between the demanding mathematical basis and practical applications in geoscience. Our method is novel because we calibrate a grounding line resolving ice sheet model in the PC space, to avoid the assumption that the difference between observation and calibration model are spatially uncorrelated (e.g. Chang et al., 2016b)). In comparison with studies that use highly aggregated quantities~~
10 ~~(like total sea level contribution (e.g. Ritz et al., 2015)), we are able to exploit more of the available observational information to add further constraints to the input parameters and sharpen the posterior distribution. Appendix B shows a calibration with total sea level contribution: the parameters are less constrained, particularly the bedrock topography and the allowable combinations of basal traction and viscosity~~

Relating climate scenarios to local ice shelf melt rates is associated with deep uncertainties itself. CMIP5 climate models are inconsistent in predicting Antarctic shelf water temperatures so that the model choice can make a substantial (>50%) difference in the increase of ocean melt by 2100 for the ASE (Naughten et al., 2018). Melt parameterisations, linking water temperature and salinity to ice melt rates, can add variations of another 50% in total melt rate for the same ocean conditions (Favier et al., 2019). The location of ocean melt can be as important as the integrated melt of an ice shelf (Goldberg et al., 2019). The treatment of melt on partially floating grid cells further impacts ice sheet models significantly, even for fine spatial
15 resolutions of 300 m (Yu et al., 2018). It is therefore very challenging to make robust climate scenario dependent ice sheet model predictions. Instead we use projections of the current state of the ASE for a well defined set of assumptions for which climate forcing uncertainty is simply represented by a halving to doubling in ocean melt.

The truncation of a principal component decomposition can cause or worsen problems related to the observations not being in the analyzed model output space (see difference in [Fig-Figure2](#)). This can mean that there is no parameter configuration θ which is a good representation of the observations. Basis rotations have been proposed to reduce this problem (Salter et al., 2018);
25 however, here we use only the portions of the observations which can be represented in the reduced PC space ([Fig-Figure 2b](#)) and argue that configurations which are able to reproduce those portions are likely to be better general representations than those configurations which cannot. We further include a discrepancy variance for each PC to account for systematic observation-model differences, including PC truncation effects and perform an initial history matching to ensure the observations are
30 reasonable close to model results.

The model perturbation has been done by amplitude scaling of the optimized input fields alone, other variations to the input fields could potentially produce model setups with better agreement to the observations (Petra et al., 2014; Isaac et al., 2015). However, computational and methodological challenges make simple scaling approaches more feasible and the use of a published dataset bars us from testing additional types of perturbations. Probabilistic calibrations are an assessment of model

setups to be the best of all tested cases. It has to be clear that this is, despite emulation, a vast simplification in searching for the best of all possible model setups imaginable.

The theoretical basis for most of the methodology used here has been laid out in Higdon et al. (2008), including the principal component decomposition, emulation and model calibration in the PC space. This calibration in basis representation has been

5 adapted and tested for general circulation (climate) and ocean models (Sexton et al., 2012; Chang et al., 2014; Salter et al., 2018; Salter and . By combining this approach with a simple but robust discrepancy representation, we attempt to bridge the gap between the demanding mathematical basis and practical applications in geoscience. We compare a novel calibration of a grounding line resolving ice sheet model in the PC space with a reprojected calibration which assumes that the difference between observations and calibration model are spatially uncorrelated (like e.g. Chang et al., 2016b). In comparison with studies that calibrate the
10 total sea level contribution (like e.g. Ritz et al., 2015), we are able to exploit more of the available observational information to add further constraints to the input parameters and sharpen the posterior distribution (Figure 4 and 5b).

A combined temporal and spatial calibration could help to use even more of the available information captured by observations in regions like the ASE where dynamic changes in the ice sheet have been observed. The temporal component could in particular help to constrain the basal sliding law exponent and ocean melt scaling.

15 6 Conclusions

We present probabilistic estimates of the dynamic contribution to sea level of the Amundsen Sea Embayment in West Antarctica over the next 50 years ~~using from~~ a grounding line resolving ice sheet model. We performed a Bayesian calibration of a published ice sheet model ensemble with satellite measurements of surface elevation changes from 1992-2015, using spatial decomposition to increase the amount of information used from the observations and emulation techniques to search the
20 parameter space more thoroughly ~~and estimate the probability distribution for sea level.~~

~~We find that the modified bedrock topography derived by Nias et al. (2016) results in quantitatively far more consistent model representation of the Amundsen Sea Embayment than Bedmap2. The calibration has been tested on synthetic test cases and can reliably constrain the bedrock, basal traction and ice viscosity amplitudes.~~ Identifying the most successful basal sliding law and ocean melt rate is more challenging, probably due to their slow impact on ice sheet behaviour ~~and compared to~~ the short
25 calibration timescale. ~~Nevertheless, we find the calibration favours higher melt rates than those derived by Nias et al. (2016) in model initialisation and a linear sliding law.~~

~~The calibration leads to a substantial reduction in the upper tail of the probability distribution of. The use of net sea level contribution, leading to quite a symmetric distribution. The predicted alone allows a wide range of parameter setups, which share the initial net mass loss. This ambiguity (weak constraint) also results in relative wide sea level contribution within
30 the next 50 years from the Amundsen Sea Embayment will most likely be between 0.6 and 23.3 mm SLE (90% probability interval) with the median and most likely model parameter configurations predicting 11.0 and 19.2 mm SLE, respectively. The calibration limits the predicted extent of grounding line retreat for Pine Island and Thwaites Glaciers, but predicts up to 28 km retreat for Smith Glacier.~~

7 Emulator regression and validation

We use Gaussian Process (GP) models for emulation and train a separate GP model for each Principal Component (PC) and time period. We use a Matern ($\frac{5}{2}$) covariance function, with the covariance function (hyper-) parameters being optimized on the marginal likelihood with five repetitions using the Python GPy module. The nugget term is set to zero, forcing the emulator to predict the exact values at training points, reflecting the deterministic nature of the probability distributions. The extra information from the use of two-dimensional calibrations adds stronger parameter constraints, showing that this method can be used to reduce uncertainties in ice sheet model. A constant mean function with $N(0, 0.5)$ prior is used, accounting for the initial centering of \tilde{Y} projections. We compare and discuss spatial calibrations in both, basis and reprojected representation.

The first 4 PCs are emulated for the calibration (first 7 years of model period) and 5 PCs are emulated for the predictions (after 10 Using satellite observations we find the modified bedrock topography derived by Nias et al. (2016) to result in quantitatively far more consistent model representation of the Amundsen Sea Embayment than Bedmap2. Compared to prior estimates, the calibrations lead to a drastic reduction in the projection uncertainty by more than 80%. Within the 50 years). This choice is based on the different decline in variance represented by PCs and ensures that 90% of the variance is covered in both cases (Fig. ??) year model period the Amundsen Sea Embayment is expected to contribute between 13.9 and 24.8 mm SLE (90% probability interval) with a most likely global sea level contribution of 18.4 mm SLE.

Variance in model ensemble ice thickness change fields explained by PCs after 7 (left) and 50 years (right). The illustrated variance scales with the eigenvalues of corresponding PCs which are the squared singular values (diagonal entities of S).

In the following we will illustrate the emulator performance by a leave-one-out (LOO) cross-validation scheme. For this we repeat all steps of the emulator setup for subsets of all but one of the full ensemble, and use that emulator to predict the PC scores of the left-out ensemble member. These are compared with the actual ice sheet model values to validate the emulator. This process is repeated until each ensemble member is left out once.

Code availability. Code can be accessed at <https://github.com/Andreas948>

Figure ?? shows the ice sheet model PC scores versus the LOO emulator prediction of the same quantity. We see an overall good correlation without serious outliers. The emulator uncertainty is assessed as well in Table ?. Around 90% of the differences between emulator and ice sheet model are within the two σ_{ω} emulator uncertainty intervals, i.e. approximately as expected (95%) for a normal distribution. The emulator performance is uniform within the parameter space (not shown).

Leave-one-out emulator validation plot for year 7 (left) and year 50 (right). Grey error bars represent $3\sigma_{\omega}$, i.e. emulator uncertainties. All $k = 4$ (left) and $k = 5$ (right) PC scores of each LOO repetition are shown together.

Emulator validation metrics Year 7 Year 50 RMSE (predicted-simulated) 3.07 4.76 RMSE (predicted-simulated)/range 0.70% 0.73% Pearson's r 0.998 0.997 Spearman's rho 0.998 0.993 Kendall tau 0.970 0.940 Fraction in 95% range 89.1% 90.5%

Appendix A: Net sea level contribution calibration

Likelihood evaluations as in Fig. 5 but using exclusively the seven-year mean rate of sea level rise contribution from the observed area for likelihood calculations. The observational uncertainty is based on the variance among the 14 observational periods and the model discrepancy σ_{ϵ}^2 is set to twice the observational variance while emulator uncertainty is neglected here

- 5 Figure ?? shows the result of calibrating with total sea level rise contribution of 0.33 mm SLE per year (McMillan et al., 2014), instead of two-dimensional surface elevation changes in the PC space as in the main analysis (Fig. 5). The parameter space is less constrained, particularly for bedrock topography, where neither choice is strongly preferred, and the combination of basal traction and viscosity, where more combinations are allowed. However, the two calibrations do not contradict each other, as there is a considerable amount of intersection in the estimates of likely parameter combinations. This demonstrates the value
- 10 of the extra information – and stronger parameter constraints – provided by the use of two-dimensional observations.

Author contributions. AW conducted the study with TE, PH and NE giving valuable advice on the study design and IN on the model data processing and interpretation. All authors contributed to the interpretation of the study results. AW prepared the manuscript with contributions from all co-authors.

Competing interests. The authors declare that they have no competing interests

- 15 *Acknowledgements.* We would like to thank Hannes Konrad for ~~shareing~~ sharing and advising on the satellite observations and Mark Brandon for general advice.

References

- Arthern, R. J. and Williams, C. R.: The sensitivity of West Antarctica to the submarine melting feedback, *Geophysical Research Letters*, 44, 2352–2359, 2017.
- Bamber, J. L., Westaway, R. M., Marzeion, B., and Wouters, B.: The land ice contribution to sea level during the satellite era, *Environmental Research Letters*, 13, 063 008, 2018.
- Bulthuis, K., Arnst, M., Sun, S., and Pattyn, F.: Uncertainty quantification of the multi-centennial response of the Antarctic ice sheet to climate change, *The Cryosphere*, 13, 1349–1380, 2019.
- Chang, W., Haran, M., Olson, R., Keller, K., et al.: Fast dimension-reduced climate model calibration and the effect of data aggregation, *The Annals of Applied Statistics*, 8, 649–673, 2014.
- Chang, W., Haran, M., Applegate, P., and Pollard, D.: Calibrating an ice sheet model using high-dimensional binary spatial data, *Journal of the American Statistical Association*, 111, 57–72, 2016a.
- Chang, W., Haran, M., Applegate, P., Pollard, D., et al.: Improving ice sheet model calibration using paleoclimate and modern data, *The Annals of Applied Statistics*, 10, 2274–2302, 2016b.
- Church, J. A., Clark, P. U., Cazenave, A., Gregory, J. M., Jevrejeva, S., Levermann, A., Merrifield, M. A., Milne, G. A., Nerem, R. S., Nunn, P. D., et al.: Sea level change, Tech. rep., PM Cambridge University Press, 2013.
- Cornford, S. L., Martin, D. F., Graves, D. T., Ranken, D. F., Le Brocq, A. M., Gladstone, R. M., Payne, A. J., Ng, E. G., and Lipscomb, W. H.: Adaptive mesh, finite volume modeling of marine ice sheets, *Journal of Computational Physics*, 232, 529–549, 2013.
- Cornford, S. L., Martin, D., Payne, A., Ng, E., Le Brocq, A., Gladstone, R., Edwards, T. L., Shannon, S., Agosta, C., Van Den Broeke, M., et al.: Century-scale simulations of the response of the West Antarctic Ice Sheet to a warming climate, 2015.
- DeConato, R. M. and Pollard, D.: Contribution of Antarctica to past and future sea-level rise, *Nature*, 531, 591, 2016.
- Edwards, T. L., Brandon, M. A., Durand, G., Edwards, N. R., Golledge, N. R., Holden, P. B., Nias, I. J., Payne, A. J., Ritz, C., and Wernecke, A.: Revisiting Antarctic ice loss due to marine ice-cliff instability, *Nature*, 566, 58, 2019.
- Favier, L., Durand, G., Cornford, S. L., Gudmundsson, G. H., Gagliardini, O., Gillet-Chaulet, F., Zwinger, T., Payne, A., and Le Brocq, A. M.: Retreat of Pine Island Glacier controlled by marine ice-sheet instability, *Nature Climate Change*, 4, 117, 2014.
- Favier, L., Jourdain, N. C., Jenkins, A., Merino, N., Durand, G., Gagliardini, O., Gillet-Chaulet, F., and Mathiot, P.: Assessment of sub-shelf melting parameterisations using the ocean–ice-sheet coupled model NEMO (v3. 6)–Elmer/Ice (v8. 3), *Geoscientific Model Development*, 12, 2255–2283, 2019.
- Fretwell, P., Pritchard, H. D., Vaughan, D. G., Bamber, J., Barrand, N., Bell, R., Bianchi, C., Bingham, R., Blankenship, D. D., Casassa, G., et al.: Bedmap2: improved ice bed, surface and thickness datasets for Antarctica, 2013.
- Gillet-Chaulet, F., Durand, G., Gagliardini, O., Mosbeux, C., Mouginot, J., Rémy, F., and Ritz, C.: Assimilation of surface velocities acquired between 1996 and 2010 to constrain the form of the basal friction law under Pine Island Glacier, *Geophysical Research Letters*, 43, 10–311, 2016.
- Gladstone, R. M., Lee, V., Rougier, J., Payne, A. J., Hellmer, H., Le Brocq, A., Shepherd, A., Edwards, T. L., Gregory, J., and Cornford, S. L.: Calibrated prediction of Pine Island Glacier retreat during the 21st and 22nd centuries with a coupled flowline model, *Earth and Planetary Science Letters*, 333, 191–199, 2012.
- Goldberg, D., Gourmelen, N., Kimura, S., Millan, R., and Snow, K.: How accurately should we model ice shelf melt rates?, *Geophysical Research Letters*, 46, 189–199, 2019.

- Golledge, N. R., Keller, E. D., Gomez, N., Naughten, K. A., Bernales, J., Trusel, L. D., and Edwards, T. L.: Global environmental consequences of twenty-first-century ice-sheet melt, *Nature*, 566, 65, 2019.
- Habermann, M., Maxwell, D., and Truffer, M.: Reconstruction of basal properties in ice sheets using iterative inverse methods, *Journal of Glaciology*, 58, 795–808, 2012.
- 5 Hein, A. S., Woodward, J., Marrero, S. M., Dunning, S. A., Steig, E. J., Freeman, S. P., Stuart, F. M., Winter, K., Westoby, M. J., and Sugden, D. E.: Evidence for the stability of the West Antarctic Ice Sheet divide for 1.4 million years, *Nature communications*, 7, 10 325, 2016.
- Higdon, D., Gattiker, J., Williams, B., and Rightley, M.: Computer model calibration using high-dimensional output, *Journal of the American Statistical Association*, 103, 570–583, 2008.
- Holden, P. B., Edwards, N., Oliver, K., Lenton, T., and Wilkinson, R.: A probabilistic calibration of climate sensitivity and terrestrial carbon change in GENIE-1, *Climate Dynamics*, 35, 785–806, 2010.
- 10 Holden, P. B., Edwards, N. R., Garthwaite, P. H., and Wilkinson, R. D.: Emulation and interpretation of high-dimensional climate model outputs, *Journal of Applied Statistics*, 42, 2038–2055, 2015.
- Holland, P. R., Bracegirdle, T. J., Dutrieux, P., Jenkins, A., and Steig, E. J.: West Antarctic ice loss influenced by internal climate variability and anthropogenic forcing, *Nature Geoscience*, 12, 718–724, 2019.
- 15 Isaac, T., Petra, N., Stadler, G., and Ghattas, O.: Scalable and efficient algorithms for the propagation of uncertainty from data through inference to prediction for large-scale problems, with application to flow of the Antarctic ice sheet, *Journal of Computational Physics*, 296, 348–368, 2015.
- Jenkins, A., Dutrieux, P., Jacobs, S., Steig, E. J., Gudmundsson, G. H., Smith, J., and Heywood, K. J.: Decadal ocean forcing and Antarctic ice sheet response: Lessons from the Amundsen Sea, *Oceanography*, 29, 106–117, 2016.
- 20 Joughin, I., Tulaczyk, S., Bamber, J. L., Blankenship, D., Holt, J. W., Scambos, T., and Vaughan, D. G.: Basal conditions for Pine Island and Thwaites Glaciers, West Antarctica, determined using satellite and airborne data, *Journal of Glaciology*, 55, 245–257, 2009.
- Joughin, I., Smith, B. E., and Schoof, C. G.: Regularized Coulomb friction laws for ice sheet sliding: Application to Pine Island Glacier, Antarctica, *Geophysical Research Letters*, 46, 4764–4771, 2019.
- Kennedy, M. C. and O’Hagan, A.: Bayesian calibration of computer models, *Journal of the Royal Statistical Society: Series B (Statistical Methodology)*, 63, 425–464, 2001.
- 25 Khazendar, A., Rignot, E., Schroeder, D. M., Seroussi, H., Schodlok, M. P., Scheuchl, B., Mouginot, J., Sutterley, T. C., and Velicogna, I.: Rapid submarine ice melting in the grounding zones of ice shelves in West Antarctica, *Nature communications*, 7, 13 243, 2016.
- Konrad, H., Gilbert, L., Cornford, S. L., Payne, A., Hogg, A., Muir, A., and Shepherd, A.: Uneven onset and pace of ice-dynamical imbalance in the Amundsen Sea Embayment, West Antarctica, *Geophysical Research Letters*, 44, 910–918, 2017.
- 30 Lenaerts, J. T., Vizcaino, M., Fyke, J., Van Kampenhout, L., and van den Broeke, M. R.: Present-day and future Antarctic ice sheet climate and surface mass balance in the Community Earth System Model, *Climate Dynamics*, 47, 1367–1381, 2016.
- Levermann, A., Winkelmann, R., Nowicki, S., Fastook, J. L., Frieler, K., Greve, R., Hellmer, H. H., Martin, M. A., Meinshausen, M., Mengel, M., et al.: Projecting Antarctic ice discharge using response functions from SeaRISE ice-sheet models, *Earth System Dynamics*, 5, 271–293, 2014.
- 35 Little, C. M., Oppenheimer, M., and Urban, N. M.: Upper bounds on twenty-first-century Antarctic ice loss assessed using a probabilistic framework, *Nature Climate Change*, 3, 654, 2013.
- MacAyeal, D. R., Bindschadler, R. A., and Scambos, T. A.: Basal friction of ice stream E, West Antarctica, *Journal of Glaciology*, 41, 247–262, 1995.

- McMillan, M., Shepherd, A., Sundal, A., Briggs, K., Muir, A., Ridout, A., Hogg, A., and Wingham, D.: Increased ice losses from Antarctica detected by CryoSat-2, *Geophysical Research Letters*, 41, 3899–3905, 2014.
- Milillo, P., Rignot, E., Rizzoli, P., Scheuchl, B., Mouginot, J., Bueso-Bello, J., and Prats-Iraola, P.: Heterogeneous retreat and ice melt of Thwaites Glacier, West Antarctica, *Science advances*, 5, eaau3433, 2019.
- 5 Naughten, K. A., Meissner, K. J., Galton-Fenzi, B. K., England, M. H., Timmermann, R., and Hellmer, H. H.: Future projections of Antarctic ice shelf melting based on CMIP5 scenarios, *Journal of Climate*, 31, 5243–5261, 2018.
- Nias, I., Cornford, S., and Payne, A.: New mass-conserving bedrock topography for Pine Island Glacier impacts simulated decadal rates of mass loss, *Geophysical Research Letters*, 45, 3173–3181, 2018.
- Nias, I., Cornford, S., Edwards, T., Gourmelen, N., and Payne, A.: Assessing uncertainty in the dynamical ice response to ocean warming in the Amundsen Sea Embayment, West Antarctica, *Geophysical Research Letters*, 46, 2019.
- 10 Nias, I. J., Cornford, S. L., and Payne, A. J.: Contrasting the modelled sensitivity of the Amundsen Sea Embayment ice streams, *Journal of Glaciology*, 62, 552–562, 2016.
- O’Hagan, A.: Bayesian analysis of computer code outputs: A tutorial, *Reliability Engineering & System Safety*, 91, 1290–1300, 2006.
- Pattyn, F.: The paradigm shift in Antarctic ice sheet modelling, *Nature communications*, 9, 2728, 2018.
- 15 Pattyn, F., Favier, L., Sun, S., and Durand, G.: Progress in numerical modeling of Antarctic ice-sheet dynamics, *Current Climate Change Reports*, 3, 174–184, 2017.
- Petra, N., Martin, J., Stadler, G., and Ghattas, O.: A computational framework for infinite-dimensional Bayesian inverse problems, Part II: Stochastic Newton MCMC with application to ice sheet flow inverse problems, *SIAM Journal on Scientific Computing*, 36, A1525–A1555, 2014.
- 20 Pollard, D., Chang, W., Haran, M., Applegate, P., and DeConto, R.: Large ensemble modeling of the last deglacial retreat of the West Antarctic Ice Sheet: comparison of simple and advanced statistical techniques, 2016.
- Pukelsheim, F.: The Three Sigma Rule, *The American Statistician*, 48, 88–91, <https://doi.org/10.1080/00031305.1994.10476030>, 1994.
- Rasmussen, C. E. and Williams, C. K.: *Gaussian processes for machine learning*, vol. 2, MIT Press Cambridge, MA, 2006.
- Rignot, E., Velicogna, I., van den Broeke, M. R., Monaghan, A., and Lenaerts, J. T. M.: Acceleration of the contribution of the Greenland and Antarctic ice sheets to sea level rise, *Geophysical Research Letters*, 38, <https://doi.org/10.1029/2011GL046583>, 2011.
- 25 Rignot, E., Mouginot, J., Morlighem, M., Seroussi, H., and Scheuchl, B.: Widespread, rapid grounding line retreat of Pine Island, Thwaites, Smith, and Kohler glaciers, West Antarctica, from 1992 to 2011, *Geophysical Research Letters*, 41, 3502–3509, 2014.
- Ritz, C., Edwards, T. L., Durand, G., Payne, A. J., Peyaud, V., and Hindmarsh, R. C.: Potential sea-level rise from Antarctic ice-sheet instability constrained by observations, *Nature*, 528, 115, 2015.
- 30 Ruckert, K. L., Shaffer, G., Pollard, D., Guan, Y., Wong, T. E., Forest, C. E., and Keller, K.: Assessing the impact of retreat mechanisms in a simple Antarctic ice sheet model using Bayesian calibration, *PLoS One*, 12, e0170 052, 2017.
- Salter, J. M. and Williamson, D. B.: Efficient calibration for high-dimensional computer model output using basis methods, *arXiv preprint arXiv:1906.05758*, 2019.
- Salter, J. M., Williamson, D. B., Scinocca, J., and Kharin, V.: Uncertainty quantification for computer models with spatial output using calibration-optimal bases, *Journal of the American Statistical Association*, pp. 1–40, 2018.
- 35 Scambos, T., Haran, T., Fahnestock, M., Painter, T., and Bohlander, J.: MODIS-based Mosaic of Antarctica (MOA) data sets: Continent-wide surface morphology and snow grain size, *Remote Sensing of Environment*, 111, 242–257, 2007.

- Scheuchl, B., Mouginot, J., Rignot, E., Morlighem, M., and Khazendar, A.: Grounding line retreat of Pope, Smith, and Kohler Glaciers, West Antarctica, measured with Sentinel-1a radar interferometry data, *Geophysical Research Letters*, 43, 8572–8579, 2016.
- Schlegel, N.-J., Seroussi, H., Schodlok, M. P., Larour, E. Y., Boening, C., Limonadi, D., Watkins, M. M., Morlighem, M., and Broeke, M. R.: Exploration of Antarctic Ice Sheet 100-year contribution to sea level rise and associated model uncertainties using the ISSM framework, *The Cryosphere*, 12, 3511–3534, 2018.
- 5 Schoof, C. and Hindmarsh, R. C.: Thin-film flows with wall slip: an asymptotic analysis of higher order glacier flow models, *Quarterly journal of mechanics and applied mathematics*, 63, 73–114, 2010.
- Sexton, D. M., Murphy, J. M., Collins, M., and Webb, M. J.: Multivariate probabilistic projections using imperfect climate models part I: outline of methodology, *Climate dynamics*, 38, 2513–2542, 2012.
- 10 Shepherd, A., Ivins, E., Rignot, E., Smith, B., Van Den Broeke, M., Velicogna, I., Whitehouse, P., Briggs, K., Joughin, I., Krinner, G., et al.: Mass balance of the Antarctic Ice Sheet from 1992 to 2017, *Nature*, 558, 219–222, 2018.
- Vernon, I., Goldstein, M., Bower, R. G., et al.: Galaxy formation: a Bayesian uncertainty analysis, *Bayesian analysis*, 5, 619–669, 2010.
- Williamson, D. B., Blaker, A. T., and Sinha, B.: Tuning without over-tuning: parametric uncertainty quantification for the NEMO ocean model, *Geoscientific Model Development*, 10, 1789–1816, 2017.
- 15 Yu, H., Rignot, E., Seroussi, H., and Morlighem, M.: Retreat of Thwaites Glacier, West Antarctica, over the next 100 years using various ice flow models, ice shelf melt scenarios and basal friction laws, *The Cryosphere*, 12, 3861–3876, 2018.